Monte Carlo method for solving a B_1 equation with complex-valued buckling in asymmetric geometries and generation of directional diffusion coefficients

Toshihiro Yamamoto[a*], Hiroki Sakamoto[b]

[a]*Institute for Integrated Radiation and Nuclear Science, Kyoto University, 2 Asashiro-Nishi, Kumatori-cho, Sennan-gun, Osaka, 590-0494, Japan*

[b]Independent author

Abstract

Direction-dependent diffusion coefficients generated using a Monte Carlo method that explicitly solves a heterogeneous B_1 equation are validated in this paper. The validation is conducted by comparing the direction-dependent neutron leakage using directional diffusion coefficients with the results of a neutron transport calculation. This paper develops a new method for critical buckling search calculation to solve a heterogeneous B_1 equation for an asymmetric unit cell in which the critical bucking has a complex value. A complex-valued critical buckling can be searched using the differential operator sampling method for estimating the sensitivity coefficients of k_{eff} with respect to the buckling. In an asymmetric unit cell, the neutron flux and the neutron current also have complex values. The real part of the neutron flux obtained by a critical buckling search calculation represents the neutron spectrum in the center portion of the finite geometry composed of the unit cells.

Keywords: Monte Carlo; B_1 equation; buckling; diffusion coefficient; reactor

1. Introduction

Generating group constants (including diffusion coefficients) for whole reactor core

* Corresponding author. Tel: +81 72 451 2414; fax: +81 72 451 2658
E-mail address: toshihiro.yamamoto223@gmail.com (T. Yamamoto)

analyses has been usually performed with deterministic core design codes. Development of the use of continuous energy Monte Carlo calculations for generating group constants has been widely performed because of its computational rigor with respect to the treatment of the geometry and neutron energy (Ilas and Rahnema, 2003; Yun and Cho, 2010; Fridman and Leppänen, 2011; Yoshioka et al., 2010; Tohjoh et al., 2005; Yamamoto, 2012; Park et al., 2012; Leppänen et al., 2016; Liu et al., 2018). Continuous energy Monte Carlo calculations are capable of generating accurate homogenized group constants for unit fuel pin cells or fuel assemblies with less approximation for the neutron spectrum and three-dimensional flux distribution. The calculations for generating group constants are usually performed with a unit fuel pin cell or a fuel assembly. In certain cases, however, several types of fuel cells or assemblies are gathered to construct a subset to take into account the interference effect between them. In the calculations for group constant generation, perfectly reflective or periodic boundary conditions are usually imposed on the outer surfaces, which implies that axial and radial neutron leakages are not considered. Because an actual reactor core has a finite dimension and is usually operated at k_{eff} =1, the neutron leakage has to be considered to generate the group constants corresponding to the operating state. One of the difficulties in the calculations is to incorporate the effect of neutron leakage that is ignored in the infinite array of a unit pin cell or a fuel assembly.

Several leakage-corrected Monte Carlo calculation techniques have been developed thus far (Gelbard and Lell, 1977; Gelbard, 1983). A method proposed by Yun and Cho (2010) introduced the effect of neutron leakage by adjusting the albedo on the outer surfaces of a fuel pin cell or a fuel assembly. During the course of a Monte Carlo criticality calculation, the albedo is updated at each cycle such that k_{eff} =1.

The present paper focuses on the B_1 method for leakage-corrected group constant generations by the Monte Carlo method. The B_1 method is generally used for representing the neutron leakage in many deterministic calculations (Duderstadt and Hamilton, 1976; Deniz,

1986; Petrovic and Benoist, 1996; Rimpault et al., 2002; Hébert, 2009; van Rooijen and Chiba, 2011; Faure and Marleau, 2017). Implementation of the B_1 method into the Monte Carlo method encounters difficulty in treating complex-valued neutron flux or neutron current. McCARD code (Shim et al., 2012; Park et al., 2012; Park et al., 2013) and Serpent code (Fridman and Leppänen, 2011; Dorval and Leppänen, 2015; Leppänen et al., 2016; Dorval, 2016a) are based on the homogeneous B_1 method for few-group constant generations. The procedure consists of two stages. First, a continuous energy Monte Carlo calculation is performed to produce fine-group homogenized cross-sections, which are subsequently used to solve the homogeneous B_1 equations. The fine-group homogenized cross sections are calculated under an environment without neutron leakage correction. Second, the homogeneous B_1 equations are solved to obtain the neutron spectrum and critical buckling corresponding to the critical state. The leakage-corrected neutron spectrum is used to generate few-group constants. The diffusion coefficients are also calculated based on the homogeneous B_1 method. This method is semi-deterministic, and the leakage-correction is not explicitly considered at the stage of the Monte Carlo calculation. The diffusion coefficients generated by the homogeneous B_1 method are isotropic and not direction-dependent. No statistical uncertainty in the fine-group Monte Carlo based cross-sections is not accounted for (nor propagated to the final few-group cross-sections). Thus, the advantage of the Monte Carlo method is not fully utilized.

The capability of calculating direction-dependent diffusion coefficients is desirable because the direction dependence of diffusion coefficients is notable in a fertile fuel assembly (Faure and Marleau, 2017) and a void containing fuel pin cell (Yamamoto, 2012). Previous works on the directional diffusion coefficients by the Monte Carlo method are based on various techniques, and they are published in Milgram (1997), Gelbard and Pego, (1979), Yamamoto (2012), Dorval and Leppänen (2015), Dorval (2016a), and Dorval (2016b). In Yamamoto (2012), the neutron transport equation for the heterogeneous B_1 method is

explicitly solved by introducing complex-valued weights in the random walk process of a Monte Carlo calculation for leakage-corrected calculations. The leakage-corrected neutron spectrum for a fuel pin cell or a fuel assembly was obtained by the Monte Carlo method during a critical buckling search calculation. The method was validated by comparing the neutron spectrum with a deterministic reactor analysis code SRAC (Okumura et al., 2007). However, the directional diffusion coefficients calculated with the Monte Carlo method were not fully validated in Yamamoto (2012) because of the lack of the reference solutions at the time of the publication. One of the objectives of the present paper is to validate the directional diffusion coefficients generated by the heterogeneous B_1 method using the Monte Carlo method.

The Monte Carlo algorithm for the heterogeneous B_1 method developed in Yamamoto (2012) has a limitation in that it can be only applied if a unit cell has a plane of symmetry. There are two reasons for that limitation. If the unit cell has a plane of symmetry, the imaginary part of the integrated flux within the unit cell vanishes due to the positive/negative symmetry of the imaginary part when the flux is integrated over the whole unit cell. Thus, the imaginary part of the fission source does not need to be considered, which makes the conventional power iteration algorithm available in an existing Monte Carlo code without any special modifications to it (Yamamoto, 2012; Yamamoto, 2013). Another reason is that as Tommasi (2015) noted, the critical buckling becomes a complex value in an asymmetric unit cell in order to obtain a real-valued k_{eff}-eigenvalue. In other words, the real and imaginary parts of the complex-valued eigenvalue need to be unity and zero, respectively, by simultaneously adjusting the real and imaginary parts of the complex-valued critical buckling. A new Monte Carlo algorithm for the critical buckling search needs to be developed to apply the B_1 method to an asymmetric unit cell, which is another objective of this paper.

The outline of this paper is briefly as follows. First, multi-group directional diffusion coefficients generated from the B_1 method that uses the Monte Carlo algorithm in Yamamoto

(2012) are used in a diffusion calculation. The neutron leakage obtained by the diffusion calculation is compared with that in the actual heterogeneous critical core with a finite dimension. How closely the diffusion calculation can reproduce the neutron transport calculation for the heterogeneous geometry will be investigated. Second, a new Monte Carlo algorithm for critical buckling search in an asymmetric unit cell is proposed, and numerical tests are performed to validate the new algorithm.

2. Monte Carlo algorithm for leakage-corrected calculation

2.1 Critical buckling search and directional diffusion coefficient in a symmetric geometry

A Monte Carlo algorithm for leakage-corrected k_{eff}-eigenvalue calculations using the B_1 method has been presented in previously published literature report (Yamamoto, 2012). In this section, the algorithm is only briefly explained, and some parts of (Yamamoto, 2012) are duplicated. In the heterogeneous B_1 method, the angular neutron flux is factorized as

$$\psi(\boldsymbol{r},\boldsymbol{\Omega},E) = \phi(\boldsymbol{r},\boldsymbol{\Omega},E)exp(i\boldsymbol{B}\cdot\boldsymbol{r}), \quad (1)$$

where $\boldsymbol{r}$= the position vector, $\boldsymbol{\Omega}$= the particle direction, E = the neutron energy, $i=\sqrt{-1}$, and $\phi(\boldsymbol{r},\boldsymbol{\Omega},E)$= the spatial fine structure of the neutron flux within a unit cell. The buckling vector $\boldsymbol{B}$ is defined as

$$\boldsymbol{B} = B_x\boldsymbol{e}_x + B_y\boldsymbol{e}_y + B_z\boldsymbol{e}_z, \quad (2)$$

where $B_i(i=x,y,z)=$ the geometric buckling in the i-direction, and $\boldsymbol{e}_i(i=x,y,z)=$ the unit vector in the i-direction. Substituting Eq. (1) into a neutron transport equation for k_{eff}-eigenvalue and dividing the equation by $exp(i\boldsymbol{B}\cdot\boldsymbol{r})$, we obtain

$$\boldsymbol{\Omega}\cdot\nabla\phi(\boldsymbol{r},\boldsymbol{\Omega},E)+\Sigma_t(\boldsymbol{r},E)\phi(\boldsymbol{r},\boldsymbol{\Omega},E)$$

$$=\int_{4\pi}d\boldsymbol{\Omega}'\int dE'\Sigma_s(\boldsymbol{r},\boldsymbol{\Omega}'\rightarrow\boldsymbol{\Omega},E'\rightarrow E)\phi(\boldsymbol{r},\boldsymbol{\Omega}',E') \tag{3}$$

$$+\frac{\chi(E)}{4\pi k_{eff}}\int_{4\pi}d\boldsymbol{\Omega}'\int dE'\nu\Sigma_f(\boldsymbol{r},E')\phi(\boldsymbol{r},\boldsymbol{\Omega}',E')\ -i\boldsymbol{B}\cdot\boldsymbol{\Omega}\phi(\boldsymbol{r},\boldsymbol{\Omega},E),$$

where Σ_t =the macroscopic total cross section, Σ_s =the macroscopic scattering cross section, Σ_f =the macroscopic fission cross section, χ =the fission neutron spectrum, and ν =the number of neutrons per fission. Eq. (3) is highly similar to the ordinary transport equation for k_{eff}-eigenvalue, except that the last term on the right-hand side is added. To solve Eq. (3) with the Monte Carlo method, the last term in Eq. (3) needs to be included during the random walk processes of the Monte Carlo calculation. There can be several ways to include this term. One is proposed by Rouchon et al. (2017). This paper adopts another way as follows. In the ordinary Monte Carlo algorithm, the particle weight remains unchanged during the free flight distance. However, in the Monte Carlo algorithm for Eq. (3), the particle weight changes continuously during the flight distance. When a particle flies a distance s_j in the *j*th flight path with a direction $\boldsymbol{\Omega}_j$, the initial weight W_j changes to

$$W_{j+1}=W_j\exp\left(-i\boldsymbol{B}\cdot\boldsymbol{\Omega}_j s_j\right)=W_j\left(\cos\left(\boldsymbol{B}\cdot\boldsymbol{\Omega}_j s_j\right)-i\cdot sin\left(\boldsymbol{B}\cdot\boldsymbol{\Omega}_j s_j\right)\right). \tag{4}$$

In the ordinary Monte Carlo algorithm, the neutron flux is obtained simply by the sum of the product of the flight distance and the particle weight ws_j if the track length estimator is used. In the algorithm for Eq. (3), however, the particle weight changes continuously. Thus, the product for the *j*th flight distance is calculated by integrating Eq. (4) with s_j:

$$TL_j=\int_0^{s_j}W_j\exp\left(-i\boldsymbol{B}\cdot\boldsymbol{\Omega}_j s_j'\right)ds_j'=W_j\frac{1-\exp\left(-i\boldsymbol{B}\cdot\boldsymbol{\Omega}_j s_j\right)}{i\boldsymbol{B}\cdot\boldsymbol{\Omega}_j}. \tag{5}$$

The flight distance is determined in the same manner as the usual Monte Carlo calculations:

$$s=-\frac{\ell n\xi}{\Sigma_t}, \tag{6}$$

where ξ = uniform pseudo random number from (0, 1). A particle with a complex weight is transported to the next collision site. At each collision site, the weight is reduced as

$$W_j' = W_j \frac{\Sigma_s}{\Sigma_t} = \mathrm{Re}[W_j] \frac{\Sigma_s}{\Sigma_t} + i \cdot \mathrm{Im}[W_j] \frac{\Sigma_s}{\Sigma_t}, \quad (7)$$

where W_j' = the weight after weight reduction at the (j−1)th collision site, Re[·] =the real part, and Im[·] = the imaginary part. The Russian roulette game is applied separately to the real and imaginary parts when either or both of $\left|\mathrm{Re}[W_j']\right|$ and $\left|\mathrm{Im}[W_j']\right|$ are less than a lower weight boundary. When either the real or imaginary part is killed but the other part survives, the particle is continually transported. Although either of the two parts is killed, it returns when the other surviving part is transported to the next collision site as can be seen in Eq. (4). The particle is killed only when both parts are killed at the same time.

At each collision point, the number of fission source points n that will be used in the next cycle is calculated as

$$n = \mathrm{Int}\left(\mathrm{Re}[W_j] \frac{\nu\Sigma_f}{\Sigma_t} + \xi\right), \quad \text{if } \mathrm{Re}[W_j] > 0, \quad (8)$$

where Int(·)= the integer part. As discussed in (Yamamoto, 2012), if the unit cell has an orthogonal symmetry plane, the imaginary part of the fission sources does not need to be stored due to the cancellation in a symmetric geometry. The determination of the fission sources in an asymmetric geometry is discussed in Sec. 2.2. In addition, as indicated in Eq. (8), the fission sources caused by a negative weight can be omitted. In (Yamamoto, 2012 and Yamamoto, 2013), it is conjectured from some numerical tests that the omission of the negative weights involves no biases. It follows that the conventional Monte Carlo algorithm for determination of the fission sources for the next cycle can be utilized for leakage-corrected calculations using the B_1 method.

k_{eff}-eigenvalue is calculated at the end of each cycle as

$$k_{eff} = \mathrm{Re}\left[\frac{1}{M}\sum_j \nu\Sigma_f \cdot TL_j\right], (\text{track length estimator}), \quad (9)$$

$$k_{eff} = \mathrm{Re}\left[\frac{1}{M}\sum_j \frac{\nu\Sigma_f}{\Sigma_t}\cdot W_j\right], \text{(collision estimator)}, \tag{10}$$

where the summation is carried out for all trajectories or all collisions within the cycle, and M= the sum of the weights of the starting particles from the fission source sites.

Suppose that the directional bucklings, B_y and B_z, are fixed and B_x is searched such that we obtain k_{eff} =1. The buckling B_x used for the next cycle is determined so that k_{eff} approaches unity as

$$B_{x,m+1} = B_{x,m} + c\left(k_{eff,m} - 1\right), \tag{11}$$

where m is the cycle number and c is an arbitrary positive value. An appropriate value for the parameter c can be easily found by several trial runs.

The directional diffusion coefficients of the gth energy group are calculated during the critical buckling search calculation as (Yamamoto, 2012)

$$D_{k,g} = \frac{1}{B_k}\frac{J_{k,g}}{\varphi_g}, \quad k = x, y, z. \tag{12}$$

φ_g and $J_{k,g}$ are calculated as follows:

$$\varphi_g = \int_{E_g}^{E_{g-1}} \sum_j \mathrm{Re}[TL_j(E)]dE, \tag{13}$$

$$J_{k,g} = \sum_j \Omega_{k,j} \int_{E_g}^{E_{g-1}} \mathrm{Im}[TL_j(E)]dE, \quad k = x, y, z, \tag{14}$$

where j is summed over all flight paths in energy band $E_g < E < E_{g-1}$ within the whole domain, and $\Omega_{k,j}$ =the direction cosine for the k-axis.

2.2 Monte Carlo method for complex-valued buckling in an asymmetric geometry

The critical buckling and the k_{eff} are both real in a critical buckling search calculation in a symmetric unit cell. For an asymmetric cell, however, the buckling that is parallel to the direction having asymmetry must be complex in order to obtain a real-valued k_{eff} (Hughes, 1979). If we persisted in the real-valued buckling in an asymmetric cell, k_{eff} would have to be

complex (Tommasi, 2015). The global flux shape corresponding to the complex-valued buckling is

$$exp(i\boldsymbol{B}^* \cdot \boldsymbol{r}) = exp(i\mathrm{Re}[\boldsymbol{B}^*] \cdot \boldsymbol{r})\, exp(-\mathrm{Im}[\boldsymbol{B}^*] \cdot \boldsymbol{r}), \quad (15)$$

where the asterisked buckling denotes a complex-valued buckling (i.e., $\boldsymbol{B}^* = \boldsymbol{B_r} + i\boldsymbol{B_i}$). The real part of the complex-valued buckling stands for the buckling of symmetric cosine distribution, and the imaginary part stands for the neutron drift in a preferred direction. When we consider a one-dimensional geometry for simplicity, the complex-valued buckling implies that the global flux shape is represented by $cos(\mathrm{Re}[B^*]x)\, exp\,(-\mathrm{Im}[B^*]x)$.

In this section, a Monte Carlo algorithm to search a complex-valued buckling corresponding to k_{eff} =1 is presented below.

At the beginning of a critical buckling search calculation, the initial guess for the fission source distribution and the geometric buckling are given. These values can all be real values, even though the converged source distribution and the buckling eventually become complex values. A particle emitted from the source site repeatedly flies and undergoes a collision until it is killed by the Russian roulette game. In the same manner as in a symmetric cell, after the flight of a distance s_j, the particle weight W_j changes to

$$W_{j+1} = W_j\, exp\left(-i\boldsymbol{B}^* \cdot \boldsymbol{\Omega}_j s_j\right)$$
$$= W_j \left(cos\left(\boldsymbol{B_r} \cdot \boldsymbol{\Omega}_j s_j\right) - i \cdot sin\left(\boldsymbol{B_r} \cdot \boldsymbol{\Omega}_j s_j\right)\right) exp\left(\boldsymbol{B_i} \cdot \boldsymbol{\Omega}_j s_j\right), \quad (16)$$

where $\boldsymbol{B_r} = \mathrm{Re}[\boldsymbol{B}^*]$ and $\boldsymbol{B_i} = \mathrm{Im}[\boldsymbol{B}^*]$. Then, the complex-valued weight is reduced by a factor of a non-absorbing probability according to Eq. (7). Whereas a fission source with a negative or imaginary weight can be omitted in a symmetric cell, these must be explicitly treated in an asymmetric cell. To determine fission sources with complex-valued weights in the following cycle, a technique dubbed as a "binning procedure" is adopted (Yamamoto, 2009). In the "binning procedure", each fissile region is divided into a large number of small bins where positive and negative weights are summed up and cancelled. This technique has been used for Monte Carlo calculations that handle complex-valued weights (Yamamoto,

2013; Yamamoto and Sakamoto, 2014; Yamamoto and Sakamoto, 2015). A region where fission reactions can occur is divided into a large number of small bins so that the flux distribution within any bin can be deemed almost flat. At each collision point in a fission region, the weight for the fission source is accumulated in the *n*th bin:

$$W_n = \sum_j \frac{\nu\Sigma_f}{\Sigma_t} W_j, \tag{17}$$

where j is summed over all collisions in the *n*th bin during one cycle and $W_j =$ the complex-valued weight that undergoes a collision in the *n*th bin. After all source particles from the fission source sites in a cycle are exhausted, the fission sources for the next cycle are determined as follows. First, the fission source in each bin is normalized:

$$W_n' = W_n \frac{M}{\sum_{n=1}^{N} |W_n|}, \tag{18}$$

where M = the nominal number of source particles per cycle, N = the number of total bins and $|W_n| = (\mathrm{Re}[W_n]^2 + \mathrm{Im}[W_n]^2)^{1/2}$. The number of source particles in the *n*th bin, m_n, is determined as

$$m_n = \mathrm{Int}\left(M \cdot \frac{|W_n|}{\sum_{n=1}^{N} |W_n|} + \xi \right), \tag{19}$$

and the weight of each source particle in the next cycle is given by W_n'/m_n. The position of each source particle is distributed randomly and uniformly within each bin.

The flowchart of the Monte Carlo algorithm for one particle history is presented in Fig. 1.

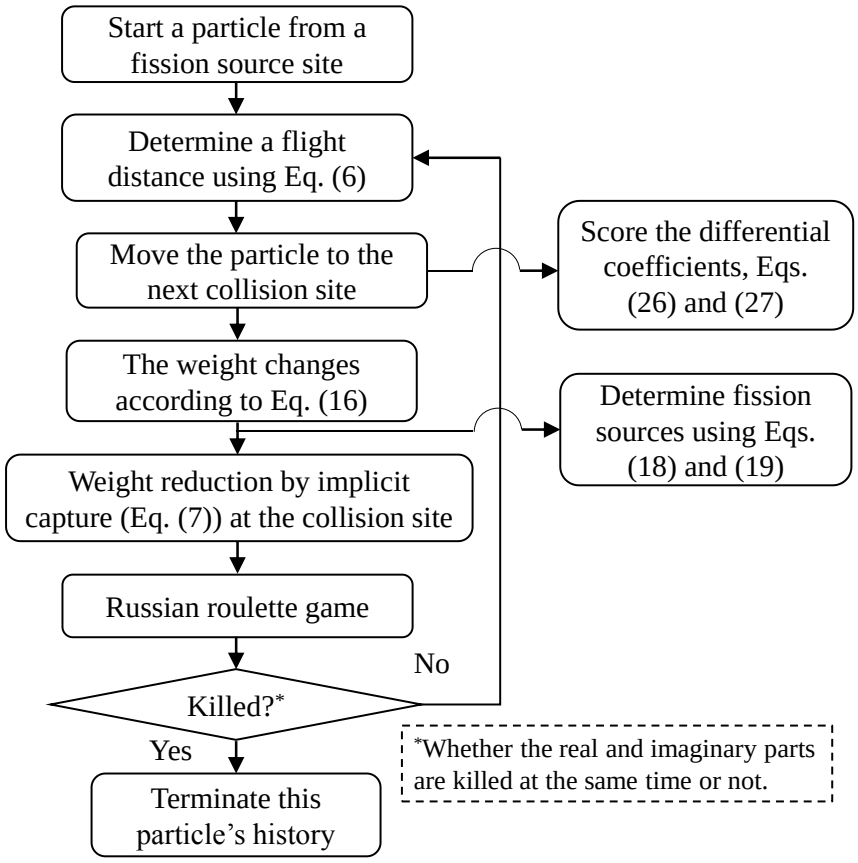

Fig. 1 Flowchart of one particle history for Monte Carlo B_1 calculation.

2.3 Critical buckling search method in an asymmetry geometry

A critical buckling can be easily searched for a symmetric cell as shown in Eq. (11). On the other hand, in a critical buckling search calculation for an asymmetric cell, the real and imaginary bucklings, $\boldsymbol{B_r}$ and $\boldsymbol{B_i}$, need to be searched simultaneously in such a way that Re[k_{eff}]= 1 and Im[k_{eff}]= 0. Let us search a complex-valued buckling only in the *x*-direction with the bucklings in the two other directions being kept constant. Suppose that we now have Re[k_{eff}] ($\neq 1$) and Im[k_{eff}] ($\neq 0$) for a tentative buckling, B_{rx} and B_{ix}. Given the sensitivity coefficients of Re[k_{eff}] and Im[k_{eff}] with respect to B_{rx} and B_{ix} and introducing a linear approximation, the corrections of B_{rx} and B_{ix} that will lead to the critical buckling are obtained by

$$\boldsymbol{A}\begin{pmatrix}\Delta B_{rx}\\ \Delta B_{ix}\end{pmatrix}+\begin{pmatrix}\mathrm{Re}[k_{eff}]\\ \mathrm{Im}[k_{eff}]\end{pmatrix}=\begin{pmatrix}1\\0\end{pmatrix}, \tag{20}$$

where $\boldsymbol{A}$ is a matrix composed of the sensitivity coefficients:

$$\boldsymbol{A} = \begin{pmatrix} \frac{\partial}{\partial B_{rx}} \mathrm{Re}[k_{eff}] & \frac{\partial}{\partial B_{ix}} \mathrm{Re}[k_{eff}] \\ \frac{\partial}{\partial B_{rx}} \mathrm{Im}[k_{eff}] & \frac{\partial}{\partial B_{ix}} \mathrm{Im}[k_{eff}] \end{pmatrix}. \tag{21}$$

At the end of each cycle, the bucklings are corrected for the next cycle as

$$B'_{rx} = B_{rx} + \Delta B_{rx}, \tag{22}$$

$$B'_{ix} = B_{ix} + \Delta B_{ix}, \tag{23}$$

where

$$\begin{pmatrix} \Delta B_{rx} \\ \Delta B_{ix} \end{pmatrix} = \boldsymbol{A}^{-1} \begin{pmatrix} 1 - \mathrm{Re}[k_{eff}] \\ -\mathrm{Im}[k_{eff}] \end{pmatrix}. \tag{24}$$

A deterministic method would require a perturbation theory to calculate the sensitivity coefficients. In the Monte Carlo method, approximate sensitivity coefficients can be easily obtained using the differential operator sampling (DOS) method (Rief, 1984; Favorite, 2002; Nagaya and Mori, 2011; Yamamoto, 2018). The DOS method is often used for estimating reactivity due to cross section changes. Yamamoto and Sakamoto (2018) recently extended the DOS to estimating the reactivity due to geometry change. This paper newly proposes a method to calculate the sensitivity coefficients of k_{eff} with respect to complex-valued buckling.

The DOS method estimates a differential coefficient of the transport or collision kernel at each flight path and collision point with respect to a perturbed parameter. When a particle moves from position $\boldsymbol{r}$ to collision point $\boldsymbol{r}'$, the transport kernel is given by

$$T(\boldsymbol{r} \to \boldsymbol{r}') = \Sigma_t exp\,(-\Sigma_t s)\, exp(-i\boldsymbol{B}^* \cdot \boldsymbol{\Omega} s)\,, \tag{25}$$

where $s = |\boldsymbol{r}' - \boldsymbol{r}|$. In ordinary Monte Carlo calculations, $exp(-i\boldsymbol{B}^* \cdot \boldsymbol{\Omega} s)$ in Eq. (25) is not included in the transport kernel. In Monte Carlo calculations for the B_1 method, this term has to be multiplied because the particle weight changes during its flight as seen in Eq. (16). The differential coefficients of the transport kernel with respect to B_{rx} and B_{ix} are, respectively,

$$\frac{1}{T}\frac{\partial}{\partial B_{rx}} T(\boldsymbol{r} \to \boldsymbol{r}') = -i\Omega_x s, \tag{26}$$

$$\frac{1}{T}\frac{\partial}{\partial B_{ix}} T(\boldsymbol{r} \to \boldsymbol{r}') = \Omega_x s. \tag{27}$$

Scoring Eqs. (26) and (27) is repeated for each flight path until the particle is discarded in terms of the Russian Roulette method. The first derivatives of the complex-valued k_{eff}-eigenvalue with respect to B_{rx} and B_{ix} for the mth particle history are respectively given by

$$\frac{\partial}{\partial B_{rx}} k_{eff,m} = \sum_j \frac{\nu\Sigma_f}{\Sigma_t} w_j S_{rj}, \tag{28}$$

$$\frac{\partial}{\partial B_{ix}} k_{eff,m} = \sum_j \frac{\nu\Sigma_f}{\Sigma_t} w_j S_{ij}, \tag{29}$$

where $w_j =$ the particle weight of the jth collision. The summation for j is carried out at every collision point during the mth history. The scores at the jth collision are

$$S_{rj} = -\sum_k i\Omega_{xk} s_k, \tag{30}$$

$$S_{ij} = \sum_k \Omega_{xk} s_k, \tag{31}$$

where the subscript k denotes the kth flight path and the summation is carried out for every flight path until the jth collision. As a result, we have the following relations of the elements in the matrix $\boldsymbol{A}$ in Eq. (21):

$$\frac{\partial}{\partial B_{rx}} \mathrm{Re}\left[k_{eff,m}\right] = \frac{\partial}{\partial B_{ix}} \mathrm{Im}\left[k_{eff,m}\right], \tag{32}$$

$$\frac{\partial}{\partial B_{rx}} \mathrm{Im}\left[k_{eff,m}\right] = -\frac{\partial}{\partial B_{ix}} \mathrm{Re}\left[k_{eff,m}\right]. \tag{33}$$

After all particles coming from the fission source sites for one cycle are exhausted, the sensitivity coefficients of k_{eff} with respect to B_{rx} and B_{ix} in the cycle are calculated as

$$\frac{\partial}{\partial B_{rx}} \mathrm{Re}\left[k_{eff}\right] = \frac{\partial}{\partial B_{ix}} \mathrm{Im}\left[k_{eff}\right] = \frac{1}{W_M} \sum_{m=1}^{M} \frac{\partial}{\partial B_{rx}} \mathrm{Re}\left[k_{eff,m}\right], \tag{34}$$

$$\frac{\partial}{\partial B_{rx}} \mathrm{Im}\left[k_{eff}\right] = -\frac{\partial}{\partial B_{ix}} \mathrm{Re}\left[k_{eff}\right] = \frac{1}{W_M} \sum_{m=1}^{M} \frac{\partial}{\partial B_{rx}} \mathrm{Im}\left[k_{eff,m}\right], \tag{35}$$

where M = the number of starting particles in one cycle and $W_M =$ the total sum of the starting particle's weights (complex value). These sensitivity coefficients obtained by Eqs. (34) and (35) are used as the elements of the matrix $\boldsymbol{A}$. B'_{rx} in Eq. (22) and B'_{ix} in Eq. (23) are used as the complex-valued buckling in the next cycle calculation. Fig. 2 shows a

flowchart of calculation in one cycle.

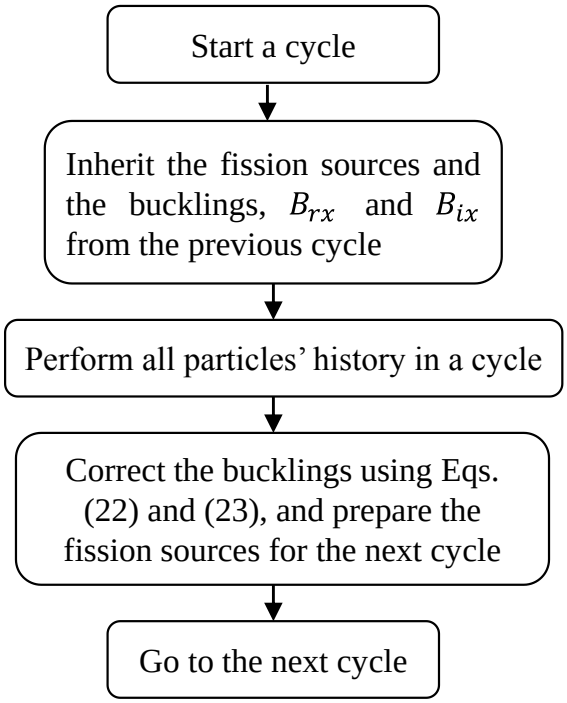

Fig. 2 Flowchart of calculation in one cycle.

A change in the buckling causes perturbations of the fission source distribution, which is not considered in Eqs. (34) and (35). Thus, the sensitivity coefficients in Eqs. (34) and (35) are approximate ones. The fission source perturbation effect is important to estimate an accurate change of k_{eff} (Nagaya and Mori, 2005; Kiedrowski, 2017; Yamamoto, 2018). The estimation of the fission source perturbation effect requires iterative calculations over several cycles. The formulation for the fission source perturbation effect is cumbersome. Then, the fission source perturbation effect is omitted in the sensitivity coefficients. While the fission source perturbation effect becomes significant for a localized perturbation, the perturbation due to the change of the buckling affects the fission source distribution uniformly over the whole domain. Thus, the source perturbation effect is considered to be minor for the sensitivity coefficients with respect to the buckling. In addition, the sensitivity coefficients are used for the correction of the buckling based on the linear approximation. Approximate sensitivity coefficients without the fission source perturbation effect are sufficient for critical

buckling search calculations.

3. Numerical tests for directional diffusion coefficient

Although the leakage-corrected calculation method using the B_1 method is already incorporated into a production-level Monte Carlo code MCNP 4C (Yamamoto, 2012), one- or two-dimensional two-energy group systems are treated using an in-house test Monte Carlo program throughout this paper.

3.1 Validation of the Monte Carlo method for the B_1 method in a symmetric cell

Before calculations for the diffusion coefficients, the critical buckling search method presented in Sec. 2.1 is validated for a symmetric cell that was used in Tommasi (2015). The one-dimensional slab geometry and the group constants are shown in Fig. 3 and Table 1, respectively. Periodic boundary conditions are imposed on the external surfaces of the slab. This slab cell is symmetric with respect to two symmetry planes as shown in Fig. 3. The critical buckling was calculated using a finite difference S_n transport code in Tommasi (2015). The critical buckling search is performed for the same problem using the Monte Carlo method. The number of histories per cycle is 80,000 and the total active cycles after skipping the initial 30 cycles are 4,000. For the "binning procedure, the entire region is equally divided into 2,100 bins where the weight cancellation is performed. The critical bucklings and k_{eff}'s obtained with the Monte Carlo method and the S_n transport code are compared in Table 2. A good agreement is achieved between the Monte Carlo method and the deterministic method. The Monte Carlo calculation is not stable for this problem because the absorber and the fuel are transparent to fast neutrons, and the flight distance of a fast neutron that flies in the vertical direction is occasionally too long in the regions. That lack of stability is why the standard deviations of the critical buckling and k_{eff} are relatively large.

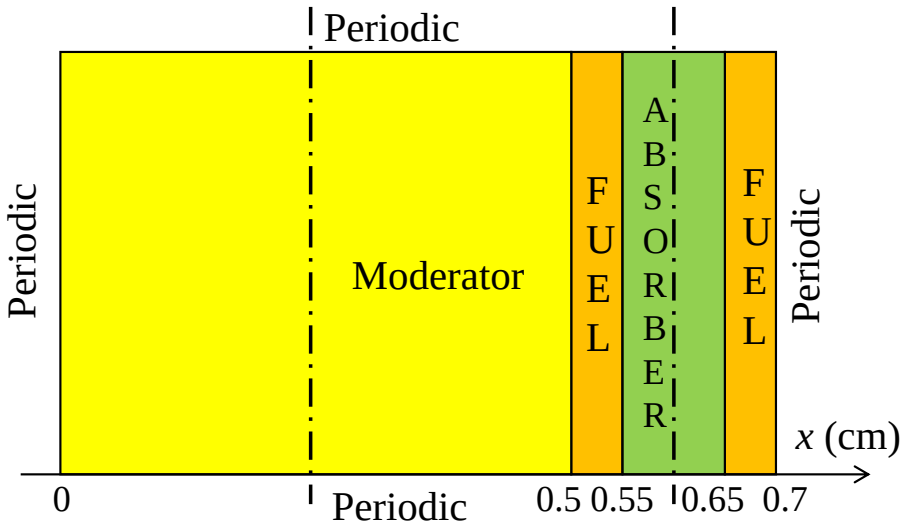

Fig. 3 Symmetric unit cell in Tommasi (2015) (The vertical dash-dot lines indicate the symmetry planes).

Table 1 Two-group constants for the one-dimensional slab (Tommasi, 2015)

		Moderator	Absorber	Fuel
Total cross section	Σ_{t1} (cm^{-1})	1.01	0.0	0.0
	Σ_{t2} (cm^{-1})	1.0	10.0	10.0
Production cross section	$\nu\Sigma_{f1}$ (cm^{-1})	0.0	0.0	0.0
	$\nu\Sigma_{f2}$ (cm^{-1})	0.0	0.0	17.365* (23.875)**
Absorption cross section	Σ_{a1} (cm^{-1})	0.0	0.0	0.0
	Σ_{a2} (cm^{-1})	0.2	10.0	10.0
Group transfer cross section	$\Sigma_s^{1\to1}$(cm^{-1})	0.01	0.0	0.0
	$\Sigma_s^{1\to2}$(cm^{-1})	1.0	0.0	0.0
Fission spectrum	χ_1	–	–	1.0
	χ_2	–	–	0.0

*for the symmetric cell in Fig. 3

**for the asymmetric cell in Fig. 6

Table 2 Critical bucklings and k_{eff} for the 1D symmetric slab.

	Buckling (cm^{-1})	Re[k_{eff}]
Monte Carlo	0.10609 ± 0.00018	0.99985± 0.00005
S_n code (Tommasi, 2015)	0.10650	0.99978

3.2 Validation of the Monte Carlo method for directional diffusion coefficients

In the numerical example in the previous section, the one-dimensional slab extends infinitely in the vertical direction and there is no leakage in the direction. In other words, the buckling in the vertical direction is zero. Another numerical example proposed in this section treats a two-dimensional square. The unit cell with a width of 1 cm is shown in Fig. 4, and the group constants are shown in Table 3. A square with a side length of 11 cm is constructed by repeating the unit cell eleven times as shown in Fig. 5. Vacuum boundary conditions are imposed on the four sides. $\nu\Sigma_{f2}$ in Table 3 is determined such that the k_{eff} of this square is as close to unity (i.e., critical) as possible. The k_{eff} of this two-dimensional 11-cell square is

1.00012 ± 0.00003.

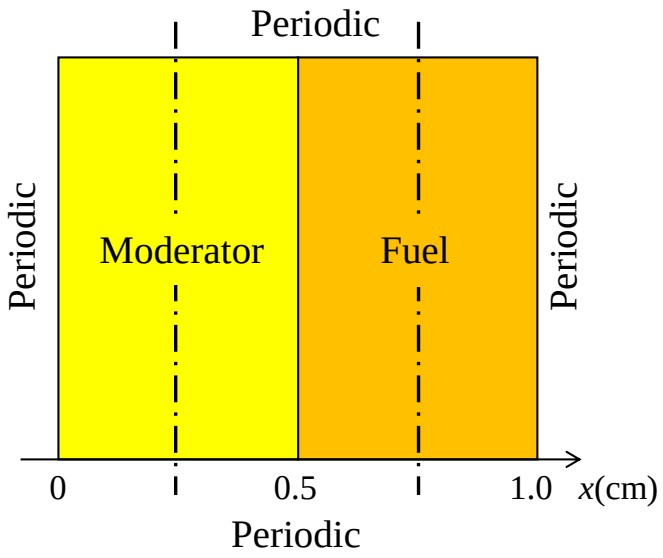

Fig. 4 Symmetric unit cell for the two-dimensional calculation (The vertical dash-dot lines indicate the symmetry planes).

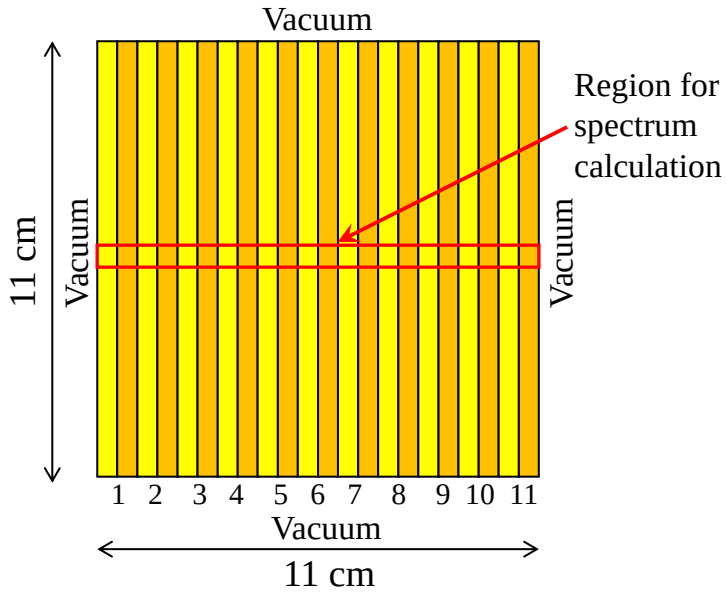

Fig. 5 Two-dimensional 11-cell square for calculating directional diffusion coefficients.

Table 3 Two-group constants for the two-dimensional square.

		Moderator	Fuel
Total cross section	Σ_{t1} (cm^{-1})	0.1	1.0
	Σ_{t2} (cm^{-1})	0.2	2.0
Production cross section	$\nu\Sigma_{f1}$ (cm^{-1})	0.0	0.0
	$\nu\Sigma_{f2}$ (cm^{-1})	0.0	0.75079
Absorption cross section	Σ_{a1} (cm^{-1})	0.0	0.07
	Σ_{a2} (cm^{-1})	0.0	0.38
Group transfer cross section	$\Sigma_s^{1\to1}$(cm^{-1})	0.06	0.651
	$\Sigma_s^{1\to2}$(cm^{-1})	0.04	0.279
Fission spectrum	χ_1	–	1.0
	χ_2	–	0.0

The critical buckling search calculation is performed for this unit cell with a fixed vertical bucking of B_y = 0.24159 (cm^{-1}). Periodic boundary conditions are imposed on all four sides. This vertical buckling is determined such that B_x is almost equal to B_y. The critical buckling in the horizontal direction obtained with the Monte Carlo calculation is 0.24154 ± 0.00002 (cm^{-1}) and k_{eff} = 1.00000 ± 0.00005. As seen in Table 3, the total cross sections of the moderator are one-tenth those of the fuel. Thus, the neutron's mean free path significantly depends on its direction, and it is anticipated that the diffusion coefficients exhibit a direction dependence. Table 4 shows the diffusion coefficients in the horizontal and vertical directions calculated with Eq. (12). The difference between the vertical and horizontal diffusion coefficients in the 2nd group is much larger than that in the 1st group. The neutron spectrum obtained by the critical buckling search calculation is considered to represent the neutron spectrum in the center of the critical core with a finite dimension. The neutron spectra are calculated in a region with a dimension of 0.5 cm × 11 cm. The region is positioned at the center in the vertical direction as shown in Fig. 5. The ratios of the flux in the 1st group to the flux in the 2nd group, ϕ_1/ϕ_2, in the moderator and fuel regions calculated with the two

methods are compared in Tables 5 and 6, respectively. The ratios calculated with the critical buckling search agree well with those in the centermost cell (Cell No. 6).

Table 4 Diffusion coefficients.

	1st group	2nd group
Horizontal (cm)	0.56954 ± 0.00008	0.29698 ± 0.00006
Vertical (cm)	0.59894 ± 0.00009	0.37262 ± 0.00008
Isotropic (cm)	0.59987 ± 0.00009	0.29993 ± 0.00008

Table 5 ϕ_1/ϕ_2 in the moderator.

Cell No.*	2D calculation	Critical buckling search
1	1.760	
2	1.415	
3	1.379	
4	1.362	
5	1.361	
6	1.357	1.357
7	1.360	
8	1.358	
9	1.362	
10	1.381	
11	1.428	

*The cell number is shown in Fig. 5.

Table 6 ϕ_1/ϕ_2 in the fuel.

Cell No.*	2D calculation	Critical buckling search
1	1.583	
2	1.479	
3	1.459	
4	1.453	
5	1.450	
6	1.448	1.448
7	1.450	
8	1.454	
9	1.460	
10	1.486	
11	1.636	

*The cell number is shown in Fig. 5.

The unit cell, which is composed of the moderator and the fuel, is homogenized using the

flux distribution calculated with the critical buckling search. The homogenized two-group constants are shown in Table 7. For comparison, the unit cell is homogenized using the flux distribution that is calculated for the infinite array of the unit cell. The homogenized two-group constants, which include no neutron leakage effect, are also shown in Table 7. Using the homogenized total cross sections, isotropic diffusion coefficients are obtained by $1/(3\Sigma_t)$. The isotropic diffusion coefficients are shown in Table 4. Using the homogenized two-group constants and the directional diffusion coefficients in Table 4, a diffusion calculation is performed for the square with a dimension of 11 cm × 11 cm. An in-house finite difference calculation code that is tailored to treat directional diffusion coefficients is used for the calculation. The number of meshes for the square is 200 × 200. The boundary condition on the external surfaces is $-D\dot{\phi}/\phi = 0.4692$, which is often used for a vacuum boundary. The objective of this diffusion calculation is to demonstrate how accurately the directional diffusion coefficients reproduce the neutron leakage obtained with a transport calculation for the direction-dependent heterogeneous configuration shown in Fig. 5. The ratios of the vertical leakage to the horizontal leakage from the outer surface are calculated with the diffusion code and the Monte Carlo code. The results are compared in Table 8. Of course, precise agreement cannot be expected between the diffusion calculation and the transport calculation. There is no criterion for judging whether the agreement is good enough. Thus, judgement should be reserved as to whether the agreement between the two methods are sufficiently good. It can be said that the direction dependency of the neutron leakage can be reproduced to some extent. The k_{eff} of the diffusion calculation for the homogenized square agrees with the transport calculation for the heterogeneous square within 0.4%. Table 8 also shows the k_{eff} calculated using the homogenized group constants without neutron leakage effect and the isotropic diffusion coefficients. The k_{eff} is overestimated by 0.88% as compared to the anisotropic diffusion calculation.

Table 7 Two-group constants for the homogenized cell.

		Critical buckling	No leakage
Total cross section	Σ_{t1} (cm^{-1})	0.56439	0.55568
	Σ_{t2} (cm^{-1})	1.0995	1.11136
Production cross section	$\nu\Sigma_{f1}$ (cm^{-1})	0.0	0.0
	$\nu\Sigma_{f2}$ (cm^{-1})	0.37520	0.38013
Absorption cross section	Σ_{a1} (cm^{-1})	0.036119	0.035442
	Σ_{a2} (cm^{-1})	0.18990	0.19240
Group transfer cross section	$\Sigma_s^{1\to1}$(cm^{-1})	0.36495	0.35923
	$\Sigma_s^{1\to2}$(cm^{-1})	0.16332	0.16101

Table 8 k_{eff} and the ratios of the vertical leakage to the horizontal leakage calculated with the three methods.

		Diffusion (anisotropic)	Monte Carlo	Diffusion (isotropic)
k_{eff}		0.99676	1.00012 ± 0.00003	1.00560
L_h/L_v	1st group	1.0467	1.0241 ± 0.0002	1.0
	2nd group	1.1421	1.1339 ± 0.0002	1.0

4. Numerical tests for the B_1 method in an asymmetric geometry

4.1 Validation of sensitivity coefficient calculations

A criticality buckling search calculation in an asymmetric cell requires estimates of sensitivity coefficients of Re[k_{eff}] and Im[k_{eff}] with respect to B_{rx} and B_{ix}. Before performing critical buckling search calculations, the DOS method for calculating sensitivity coefficients, which is defined in Eqs. (34) and (35), is validated. The test problem in Tommasi (2015) is used again in this paper. The geometry of the problem is shown in Fig. 6. This problem was originally proposed by Gelbard and Lell (1977). The group constants in Fig. 6 are the same as in Table 1, except for ν. $\nu\Sigma_{f2}$ for this problem is also listed in Table 1. This problem has no symmetry plane as seen in Fig. 6. Reference solutions for the sensitivity coefficients to be compared with the DOS method are obtained by calculating the difference

of Re[k_{eff}] and Im[k_{eff}] for slightly perturbed B_{rx}. Figs. 7 and 8 show ΔRe[k_{eff}] and ΔIm[k_{eff}] as a function of ΔB_{rx}. The reference sensitivity coefficients are obtained by linear fitting as shown in Figs. 7 and 8. In Table 9, the sensitivity coefficients by the DOS method are compared with the references. Note that the DOS method neglects the fission source perturbation effect and the reference solutions are based on the linear approximation. It is found that Re[k_{eff}] and Im[k_{eff}] are not as sensitive to B_{ix} and B_{rx} respectively as to B_{rx} and B_{ix}. In other words, $\partial \mathrm{Re}[k_{eff}]/\partial B_{ix}$ and $\partial \mathrm{Im}[k_{eff}]/\partial B_{rx}$ are much smaller than $\partial \mathrm{Re}[k_{eff}]/\partial B_{rx}$ and $\partial \mathrm{Im}[k_{eff}]/\partial B_{ix}$. Although the reference solution of $\partial \mathrm{Re}[k_{eff}]/\partial B_{ix}$ or $\partial \mathrm{Im}[k_{eff}]/\partial B_{rx}$ has a larger statistical uncertainty because of its smallness, the DOS method agrees with the reference within the statistical uncertainty. Additionally, $\partial \mathrm{Re}[k_{eff}]/\partial B_{rx}$ or $\partial \mathrm{Im}[k_{eff}]/\partial B_{ix}$ agrees well with the reference solution. In conclusion, sensitivity coefficients calculated with the DOS method can be utilized for a complex-valued buckling search calculation in an asymmetric cell.

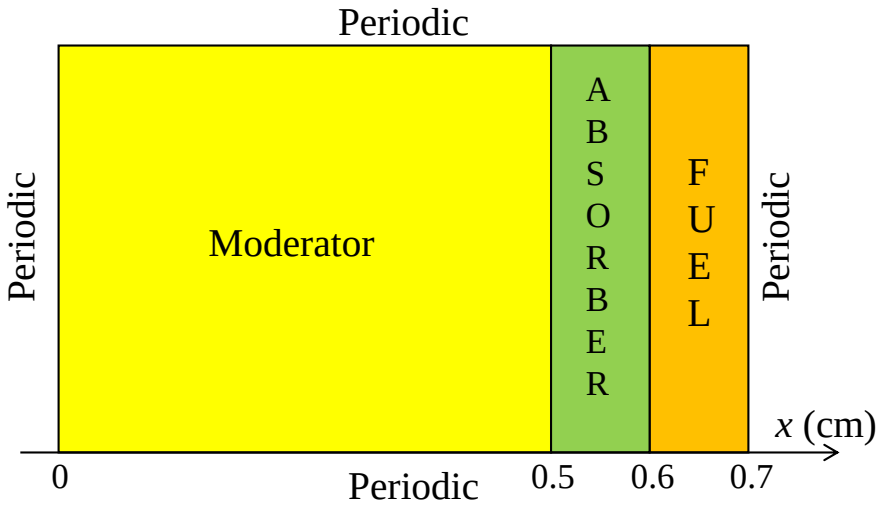

Fig. 6 Asymmetric unit cell in Tommasi (2015).

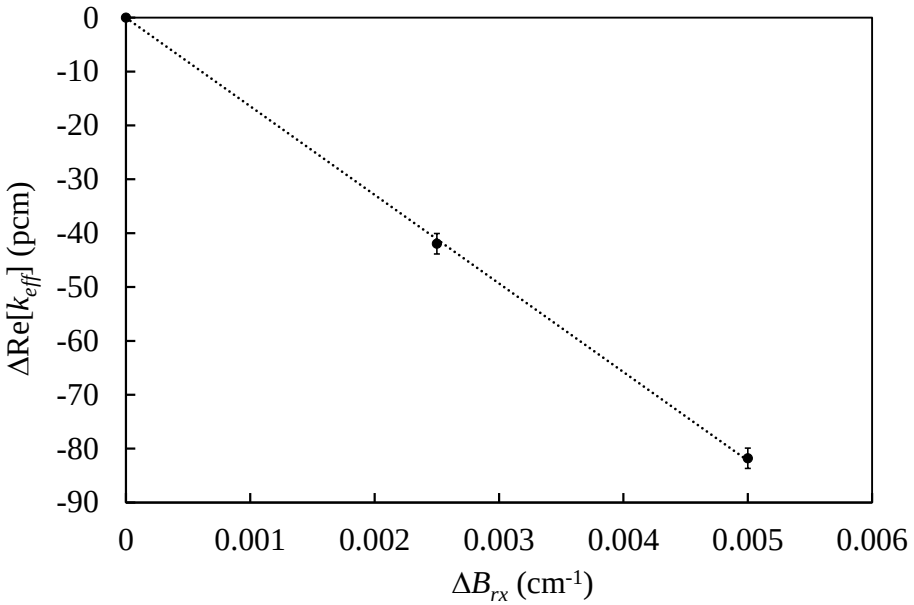

Fig. 7 ΔRe[k_{eff}] as a function of ΔB_{rx} in the asymmetric cell.

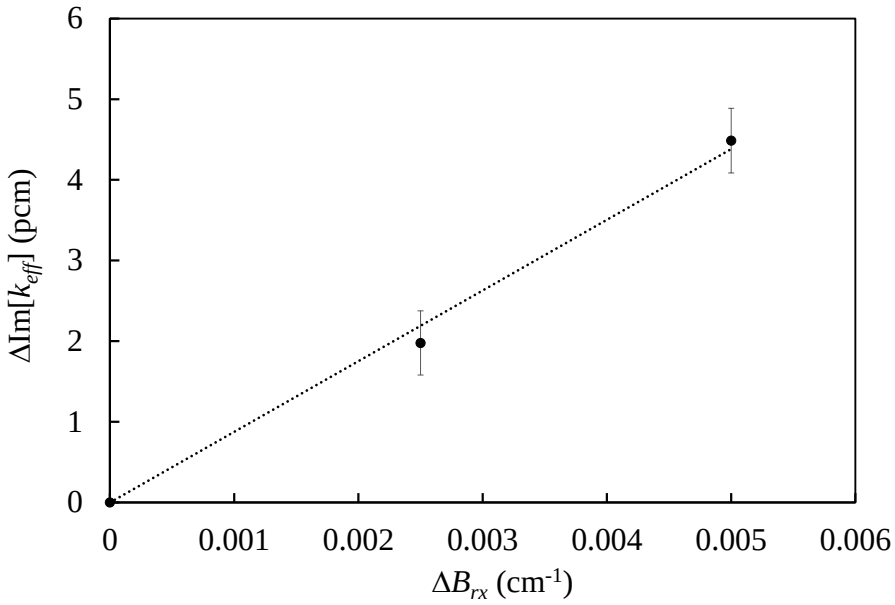

Fig. 8 ΔIm[k_{eff}] as a function of ΔB_{rx} in the asymmetric cell.

Table 9 Sensitivity coefficients calculated by DOS and linear fitting.

	DOS	Reference
$\frac{\partial}{\partial B_{rx}}\mathrm{Re}[k_{eff}], \frac{\partial}{\partial B_{ix}}\mathrm{Im}[k_{eff}]$	−0.16295 ± 0.00005	−0.1635 ± 0.0038
$\frac{\partial}{\partial B_{rx}}\mathrm{Im}[k_{eff}], -\frac{\partial}{\partial B_{ix}}\mathrm{Re}[k_{eff}]$	0.00815 ± 0.00003	0.00897 ± 0.0081

Using the technique in Sec. 2.3, a complex-valued critical buckling search calculation is performed for the asymmetric cell shown in Fig. 6. The complex-valued buckling and k_{eff} are listed in Table 10. Reference values calculated with the deterministic method in Tommasi (2015) are presented for comparison. The newly proposed Monte Carlo method precisely reproduces the complex-valued critical buckling in Tommasi (2015).

Table 10 Critical bucklings and k_{eff} for the 1D asymmetric slab in Tommasi (2015).

	B_{rx} (cm^{-1})	B_{ix} (cm^{-1})	Re[k_{eff}]	Im[k_{eff}]
Monte Carlo	0.10689 ± 0.00013	−0.14566 ± 0.00003	0.99994 ± 0.00006	0.00004 ± 0.00001
S_n code (Tommasi, 2015)	0.10703	−0.14870	0.99978	−0.00046

4.2 Leakage-corrected spectrum calculation in an asymmetric cell

As mentioned in Sec. 3.1, the numerical example in the previous section is unstable for the neutron flux calculation because it has a transparent material for fast neutrons. Then, another asymmetric one-dimensional cell is proposed for the numerical test in this section. The unit cell is composed of moderator, absorber, and fuel materials, with each having a thickness of 0.2 cm, as shown in Fig. 9. A one-dimensional slab whose width is 6.6 cm is constructed by repeating the unit cell eleven times as shown in Fig. 10. A vacuum boundary condition is imposed on the left and right surfaces. The slab is vertically infinite, and a periodic boundary condition is imposed on the upper and lower surfaces. The group constants of the materials are shown in Table 11. $\nu\Sigma_{f2}$ is determined such that the k_{eff} of this

one-dimensional finite system is equal to unity. The k_{eff} of this slab calculated with the Monte Carlo method is 0.999948 ± 0.000053. The flux distribution in this slab is shown in Fig. 11. A neutron drift in the left direction that is introduced due to the asymmetry of the unit cell is clearly observed in Fig. 11. The critical buckling search calculation for this asymmetric cell is performed to obtain the complex-valued critical buckling and the k_{eff}-eigenvalue, and they are given in Table 12. In such an asymmetric unit cell, the flux and the current obtained by a critical buckling search calculation are complex. A question arises as to what the real and imaginary parts of the flux or the current represent. In Tables 13, 14, and 15, the flux ratio of the real part of the flux, $\mathrm{Re}[\phi_1]/\mathrm{Re}[\phi_2]$, in each region is compared with the flux ratio in the one-dimensional finite slab. The ratio, ϕ_1/ϕ_2, varies with position in the slab. The variation is particularly notable in the absorber. Tables 13, 14, and 15 indicate that the flux ratio, $\mathrm{Re}[\phi_1]/\mathrm{Re}[\phi_2]$, reproduces well the flux ratio, ϕ_1/ϕ_2, in the centermost cell (Cell No. 6) of the finite slab. The results suggest that the neutron spectrum in the center of a critical core is reproduced by the critical buckling search calculation for the unit cell and that the real part of the complex-valued flux represents the product of the global flux shape, $\cos(B_{rx}x)\exp(-B_{ix}x)$, and the local flux shape.

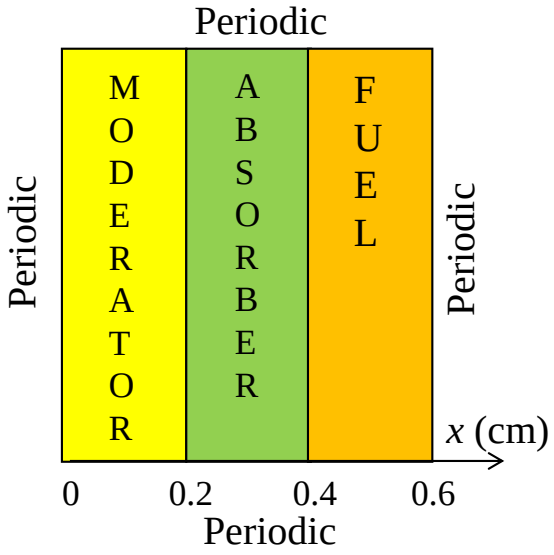

Fig. 9 Asymmetric unit cell for the test problem.

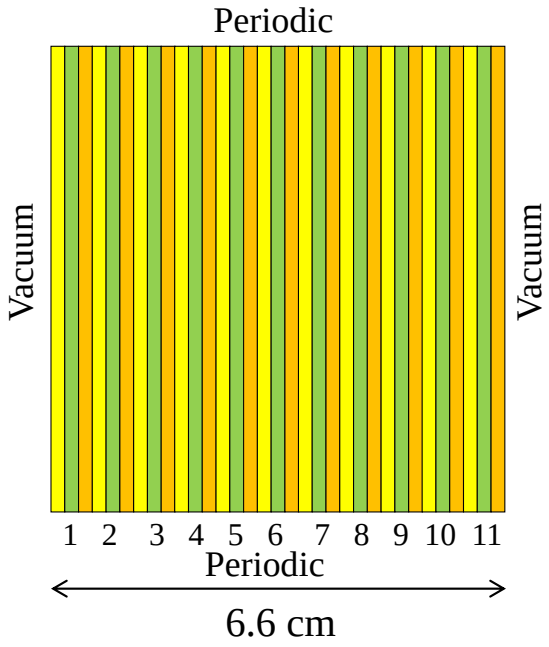

Fig. 10 One-dimensional finite slab composed of the unit cell in Fig. 9.

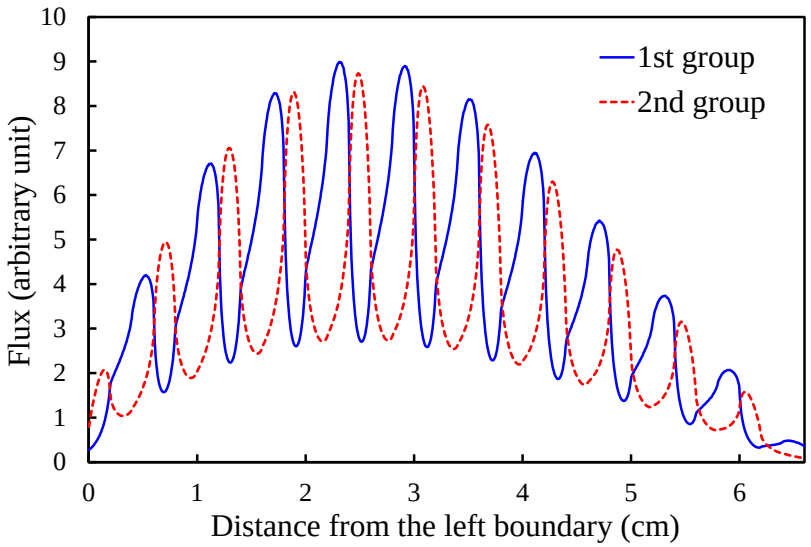

Fig. 11 Flux distributions in the one-dimensional finite slab.

Table 11 Two-group constants for the 1D asymmetric slab in Sec. 4.2.

		Moderator	Absorber	Fuel
Total cross section	Σ_{t1} (cm^{-1})	5.0	1.0	1.0
	Σ_{t2} (cm^{-1})	10.0	3.0	3.0
Production cross section	$\nu\Sigma_{f1}$ (cm^{-1})	0.0	0.0	0.0
	$\nu\Sigma_{f2}$ (cm^{-1})	0.0	0.0	5.0127
Absorption cross section	Σ_{a1} (cm^{-1})	0.0	0.2	0.0
	Σ_{a2} (cm^{-1})	0.0	3.0	2.0
Group transfer cross section	$\Sigma_s^{1\to1}$(cm^{-1})	0.0	0.8	1.0
	$\Sigma_s^{1\to2}$(cm^{-1})	5.0	0.0	0.0
Fission spectrum	χ_1	–	–	1.0
	χ_2	–	–	0.0

Table 12 Critical bucklings and k_{eff} for the asymmetric unit cell.

B_{rx} (cm^{-1})	0.45154 ± 0.00010
B_{ix} (cm^{-1})	0.15551 ± 0.00004
Re[k_{eff}]	0.999983 ± 0.000029
Im[k_{eff}]	0.000005 ± 0.000011

Table 13 ϕ_1/ϕ_2 in the moderator.

Cell No.*	1D calculation	Critical buckling search
	ϕ_1/ϕ_2	Re[ϕ_1]/Re[ϕ_2]
1	0.4221	
2	0.4486	
3	0.4466	
4	0.4456	
5	0.4451	
6	0.4446	0.4444
7	0.4440	
8	0.4436	
9	0.4428	
10	0.4419	
11	0.4440	

*The cell number is shown in Fig. 10.

Table 14 ϕ_1/ϕ_2 in the absorber.

Cell No.*	1D calculation ϕ_1/ϕ_2	Critical buckling search $\mathrm{Re}[\phi_1]/\mathrm{Re}[\phi_2]$
1	2.141	
2	1.900	
3	1.818	
4	1.775	
5	1.741	
6	1.713	1.720
7	1.684	
8	1.651	
9	1.600	
10	1.512	
11	1.204	

*The cell number is shown in Fig. 10.

Table 15 ϕ_1/ϕ_2 in the fuel.

Cell No.*	1D calculation ϕ_1/ϕ_2	Critical buckling search $\mathrm{Re}[\phi_1]/\mathrm{Re}[\phi_2]$
1	2.227	
2	2.253	
3	2.264	
4	2.270	
5	2.275	
6	2.281	2.274
7	2.288	
8	2.293	
9	2.303	
10	2.334	
11	3.295	

*The cell number is shown in Fig. 10.

5. Conclusions

This paper proposes the implementation of the B_1 method into the Monte Carlo method, which is one of the Monte Carlo techniques for generating group constants, including diffusion coefficients. The proposed method is featured by generating leakage-corrected directional diffusion coefficients. In the numerical test of this paper, leakage-corrected

horizontal and vertical diffusion coefficients that are generated with the critical buckling search calculation are used for the diffusion calculation in a two-dimensional geometry. The directional dependence of the neutron leakage is well reproduced by using the direction-dependent diffusion coefficients. The Monte Carlo technique with the B_1 method implemented can be an effective tool for generating diffusion coefficients and other group constants that will subsequently be used for full core calculations.

A critical buckling in a unit cell where the symmetry operation changes the buckling vector $\boldsymbol{B}$ to $\boldsymbol{B}$ or $-\boldsymbol{B}$ can be real value; otherwise it has to be complex as noted in previous studies. The critical buckling search calculation in an asymmetric unit cell needs to search the real and imaginary parts of the complex-valued buckling at the same time. A new Monte Carlo perturbation method for calculating the sensitivity coefficients of k_{eff} with respect to the buckling is proposed for a critical buckling search calculation. The new method uses the differential operator sampling method for calculating the sensitivity coefficients. The leakage-corrected neutron spectrum obtained by a B_1 calculation represents the spectrum in the center portion of the finite system that is composed of the repeated unit cells. In an asymmetric unit cell, the neutron flux and the current integrated over the domain are complex. The neutron spectrum in the center portion is represented by the real part of the neutron flux obtained by the critical buckling search calculation.

Future research and development will focus on the theory of how to define diffusion coefficients in an asymmetric cell, which has not been established to date. The method proposed in this paper requires the "binning procedure" to determine the complex-valued weights and positions of fission source for the next cycle as discussed in Sec. 2.2. A new technique not requiring the "binning procedure" should be developed to enhance the availability of this method so that it can be easily implemented into a variety of Monte Carlo codes.

References

Deniz, V.C., 1986. The theory of neutron leakage in reactor lattices. The CRC Handbook of Nuclear Reactor Calculations, Vol. 2. CRC Press, Boca Raton, Florida, USA, pp. 409–504.

Dorval, E., 2016a. Directional diffusion coefficients and leakage-corrected discontinuity factors: implementation in Serpent and tests. Ann. Nucl. Energy 87, 101–112.

Dorval, E., 2016b. A comparison of Monte Carlo methods for neutron leakage at assembly level. Ann. Nucl. Energy 87, 591–600.

Dorval, E., Leppänen, J., 2015. Monte Carlo current-based diffusion coefficients: application to few-group constants generation in Serpent. Ann. Nucl. Energy 78, 104–116.

Duderstadt, J.J., Hamilton, L.J., 1976. Nuclear Reactor Analysis. John Wiley & Sons, New York.

Faure, B., Marleau, G., 2017. Simulation of a sodium fast core: Effect of B_1 leakage models on group constant generation. Ann. Nucl. Energy 99, 484–494.

Favorite, J.A., 2002. An alternative implementation of the differential operator (Taylor series) perturbation methods for Monte Carlo criticality problems, Nucl. Sci. Eng. 142, 327–341.

Fridman, E., Leppänen, J., 2011. On the use of the Serpent Monte Carlo code for few-group cross section generation. Annals of Nuclear Energy, 38, 1399–1405.

Gelbard, E.M., Lell, R. 1977. Monte Carlo treatment of fundamental-mode neutron leakage in the presence of voids. Nuclear Science and Engineering, 63, 9–23.

Gelbard, E.M., Pego, R., 1979. Monte Carlo computation of directional diffusion coefficients. Proc. American Nuclear Society Topical Meeting on Computational Methods in Nuclear Engineering, Williamsburg, VA, USA, April 23–25, 1979.

Gelbard, E.M., 1983. Streaming in lattices. Advances in Nuclear Science and Technology, 15, 223–400.

Hébert, A., 2009. Applied reactor physics. Presses internationales Polytechnique.

Hughes, R.P., 1979. Complex buckling modes in asymmetric cell lattices. Nucl. Sci. Eng. 69,

430–441.

Ilas, G., Rahnema, F., 2003. A Monte Carlo based nodal diffusion model for criticality analysis of spent fuel storage lattices. Annals of Nuclear Energy, 30, 1089–1108.

Kiedrowski, B.C., 2017. Review of early 21st-century Monte Carlo perturbation and sensitivity techniques for k-eigenvalue radiation transport calculations, Nucl. Sci. Eng. 185, 426–444.

Leppänen, J., Pusa, M., Fridman, E., 2016. Overview of methodology for spatial homogenization in the Serpent 2 Monte Carlo code. Ann. Nucl. Energy 96, 126–136.

Liu, Z., Smith, K., Forget, B., Ortensi, J., 2018. Cumulative migration method for computing rigorous diffusion coefficients and transport cross sections from Monte Carlo, Ann. Nucl. Energy 112, 507–516.

Milgram, M.S., 1997. Estimation of axial diffusion processes by analog Monte Carlo: theory, tests and examples. Ann. Nucl. Energy 24, 671–704.

Nagaya, Y., Mori, T., 2005. Impact of perturbed fission source on the effective multiplication factor in Monte Carlo perturbation calculations, J. Nucl. Sci. Technol., 42, 428–441.

Nagaya, Y., Mori, T., 2011. Estimation of sample reactivity worth with differential operator sampling method, Prog. Nucl. Sci. Technol., 2, 842–850.

Okumura, K., Kugo, T., Kaneno K, Tsuchihashi, K., 2007. SRAC2006: A comprehensive neutronics calculation code system. JAEA-Data/Code 2007-004.

Park, H. J., Shim, H. J., Joo, H. G., Kim, C. H., 2012. Generation of few-group diffusion theory constants by the Monte Carlo code McCARD. Nucl. Sci. Eng. 172, 66–77.

Park, H. J., Shim, H. J., Joo, H. G., Kim, C. H., 2013. Uncertainty quantification of few-group diffusion theory constants generated by the B_1 theory-augmented Monte Carlo method. Nucl. Sci. Eng. 175, 28–43.

Petrovic, I., Benoist, P., 1996. BN Theory: Advances and New Models for Neutron Leakage Calculation. Advances in Nuclear Science and Technology 24, 223–279.

Rief, H., 1984. Generalized Monte Carlo perturbation algorithms for correlated sampling and a second-order Taylor series approach. Ann. Nucl. Energy 11, 455–476.

Rimpault, G., Plisson, D., Tommasi, J., Jacqmin, R., Rieunier, J., Verrier, D., Biron, D., 2002. The ERANOS code and data system for fast reactor neutronics analyses. Proc. Int. Conf. PHYSOR 2002, Seoul, Korea, October 7–10, 2002.

Rouchon, A., Zoia, A., Sanchez, R., 2017. A new Monte Carlo method for neutron nosie calculations in the frequency domain. Ann. Nucl. Energy 102, 465–475.

van Rooijen, W.F.G., Chiba, G., 2011. Diffusion coefficients for LMFBR cells calculated with MOC and Monte Carlo. Ann. Nucl. Energy 38, 133–144.

Shim, H.J., Han, B.S., Jung, J.S., Park, H.J., Kim, C.H., 2012. McCARD: Monte Carlo code for advanced reactor design and analysis, Nucl. Eng. Technol., 44, 161–176.

Tohjoh, M., Watanabe, M., Yamamoto, A., 2005. Application of continuous-energy Monte Carlo code as a cross-section generator of BWR core calculation. Ann. Nucl. Energy 32, 857–875.

Tommasi, J., 2015. Heterogeneous B_N equations and symmetries. Ann. Nucl. Energy 85, 145–158.

Yamamoto, T., 2009. Convergence of the second eigenfunction in Monte Carlo power iteration. Annals of Nuclear Energy, 36, 7–14.

Yamamoto, T., 2012. Monte Carlo method with complex weights for neutron leakage-corrected calculations and anisotropic diffusion coefficient. Ann. Nucl. Energy 50, 141–149.

Yamamoto, T., 2013. Improvements and new findings in Monte Carlo method with complex-valued weights for neutron leakage-corrected assembly calculations. Proc. SNA + MC 2013 - Joint Int. Conf. on Supercomputing in Nucl. Applications + Monte Carlo. Paris, France, Oct. 27–31, 2013. http://dx.doi.org/10.1051/snamc/201405312.

Yamamoto, T., Sakamoto, H., 2014. A new concept of Monte Carlo kinetics parameter

calculation using complex-valued perturbation. Ann. Nucl. Energy 71, 480–488.

Yamamoto, T., Sakamoto, H., 2015. Dynamic Monte Carlo calculation method by solving frequency domain transport equation using the complex-valued weight Monte Carlo method. Ann. Nucl. Energy 85, 426–433.

Yamamoto, T., 2018. Eigenvalue sensitivity analysis capabilities with the differential operator method in the superhistory Monte Carlo method. Ann. Nucl. Energy 112, 150–157.

Yamamoto, T., Sakamoto, H., 2018. Monte Carlo perturbation methods using "virtual density" theory for calculating reactivity due to geometry change. Ann. Nucl. Energy 119, 362–373.

Yoshioka, K., Ando, Y., 2010. Multigroup scattering matrix generation method using weight-to-flux ratio based on a continuous energy Monte Carlo technique. Journal of Nuclear Science and Technology, 47, 908–916.

Yun, S., Cho, N.Z., 2010. Monte Carlo depletion under leakage-corrected critical spectrum via albedo search. Nuclear Engineering and Technology, 42, 271–278.

Figure

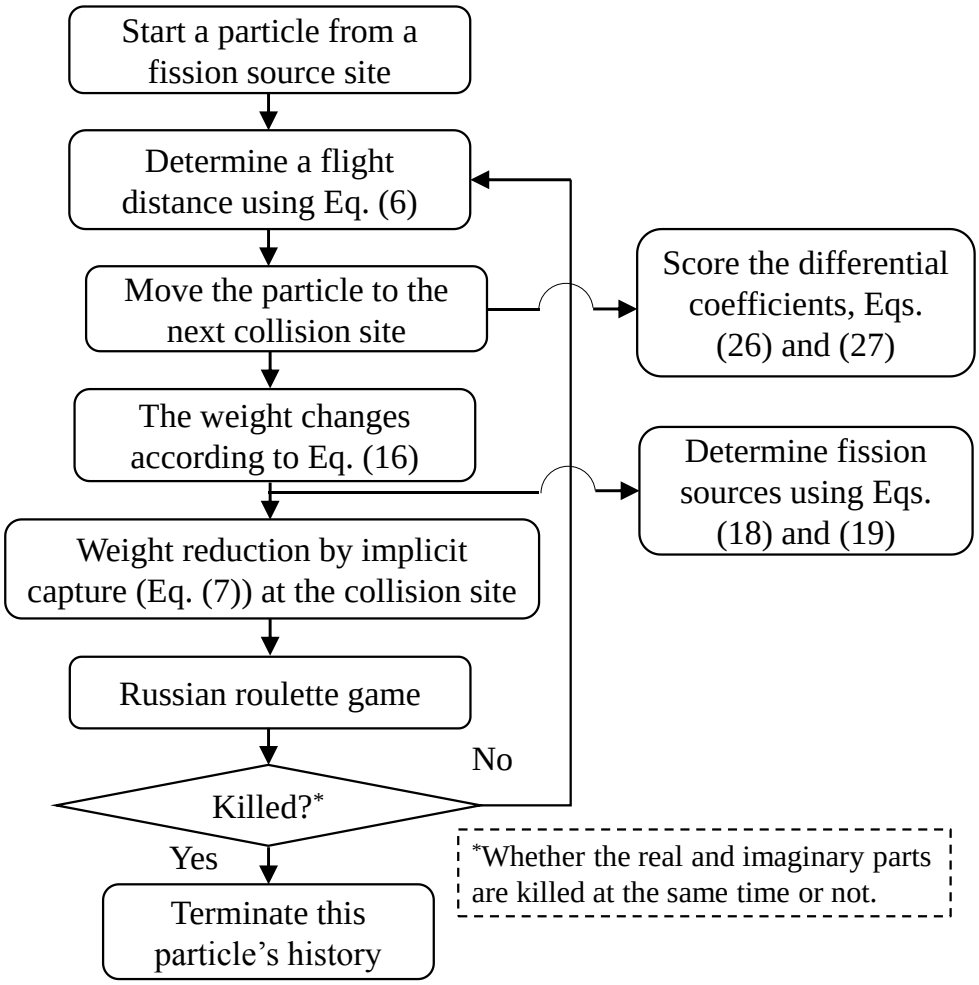

Fig. 1 Flowchart of one particle history for Monte Carlo B_1 calculation.

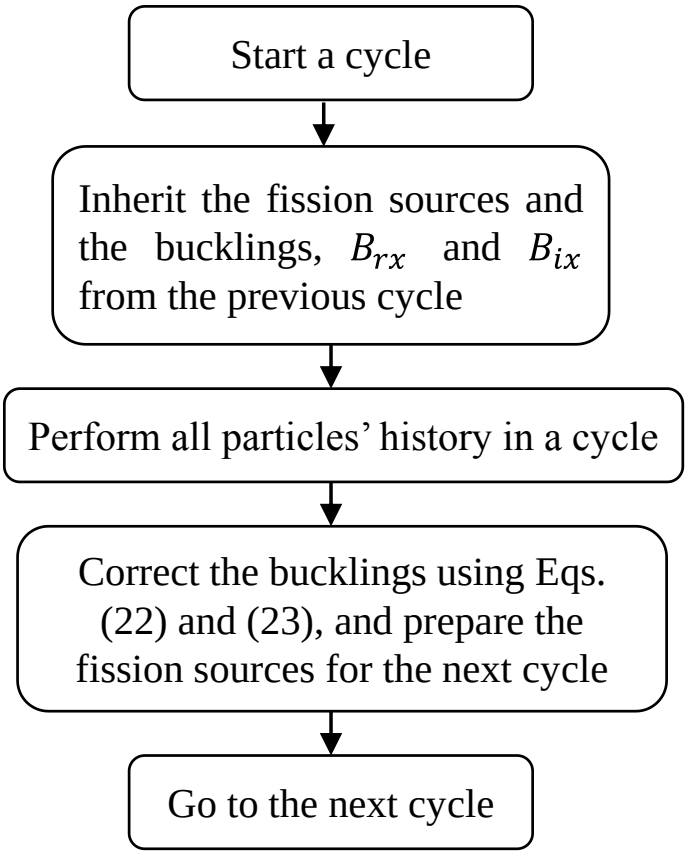

Fig. 2 Flowchart of calculation in one cycle.

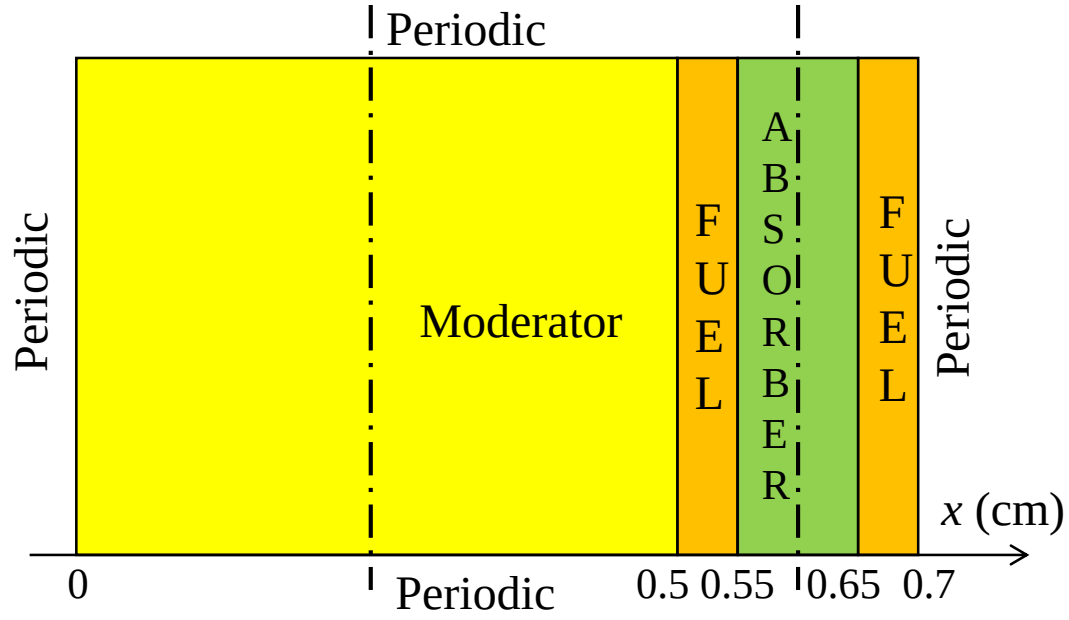

Fig. 3 Symmetric unit cell in Tommasi (2015) (The vertical dash-dot lines indicate the symmetry planes).

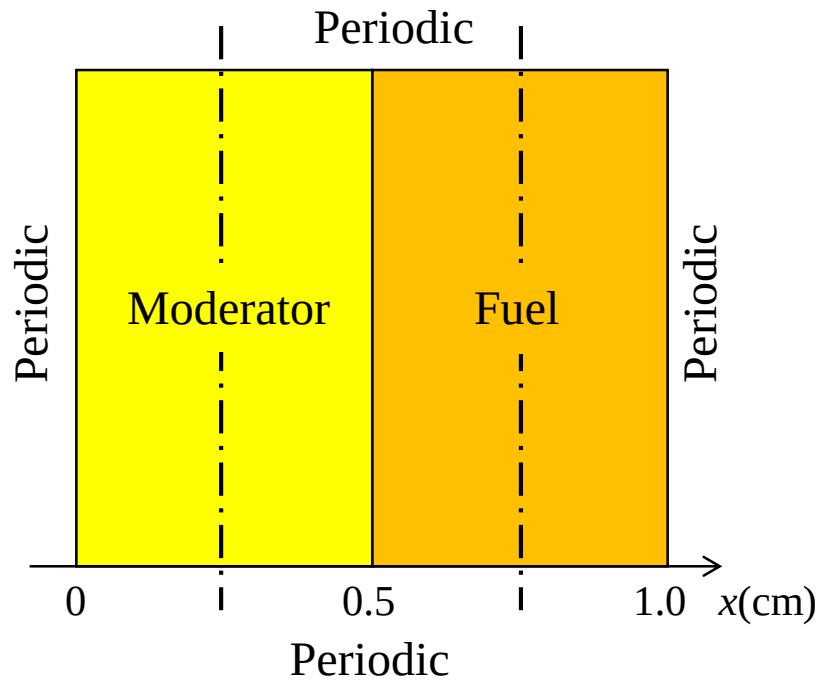

Fig. 4 Symmetric unit cell for the two-dimensional calculation (The vertical dash-dot lines indicate the symmetry planes).

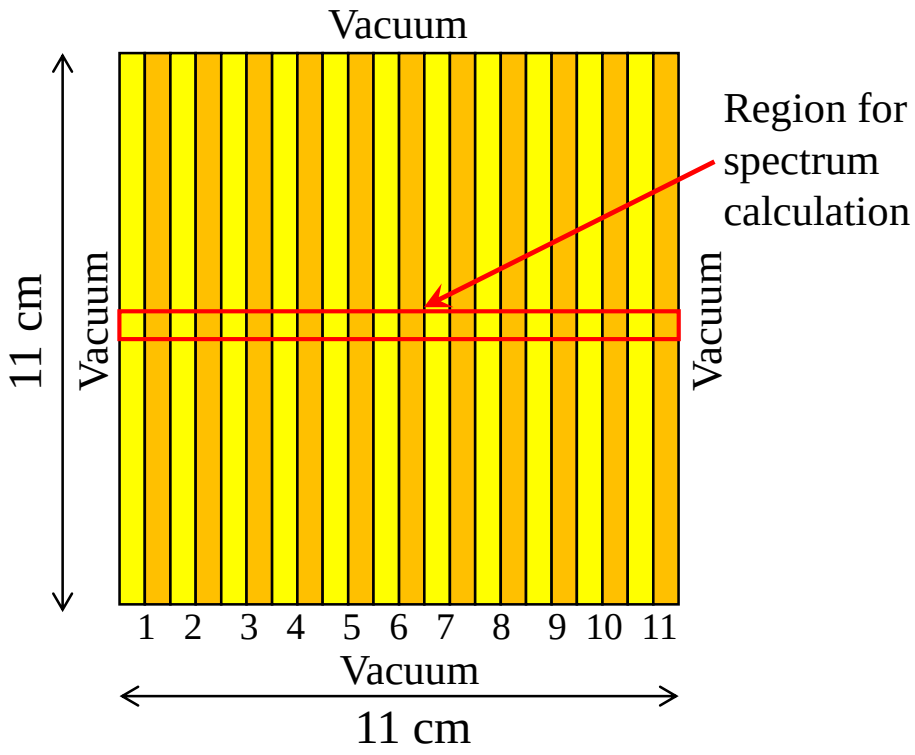

Fig. 5 Two-dimensional 11-cell square for calculating directional diffusion coefficients.

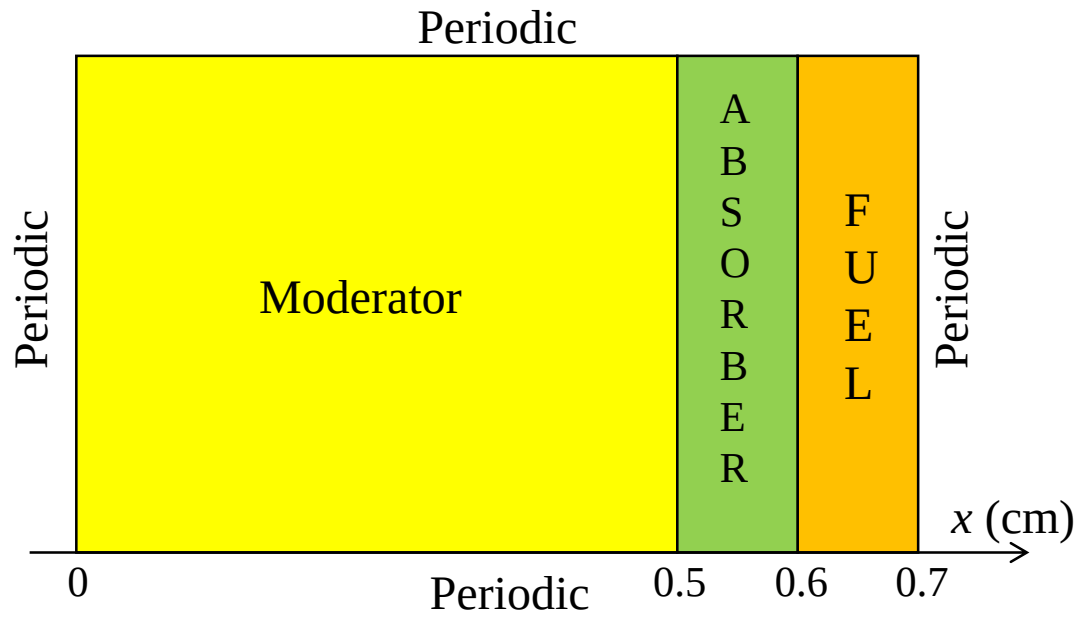

Fig. 6 Asymmetric unit cell in Tommasi (2015).

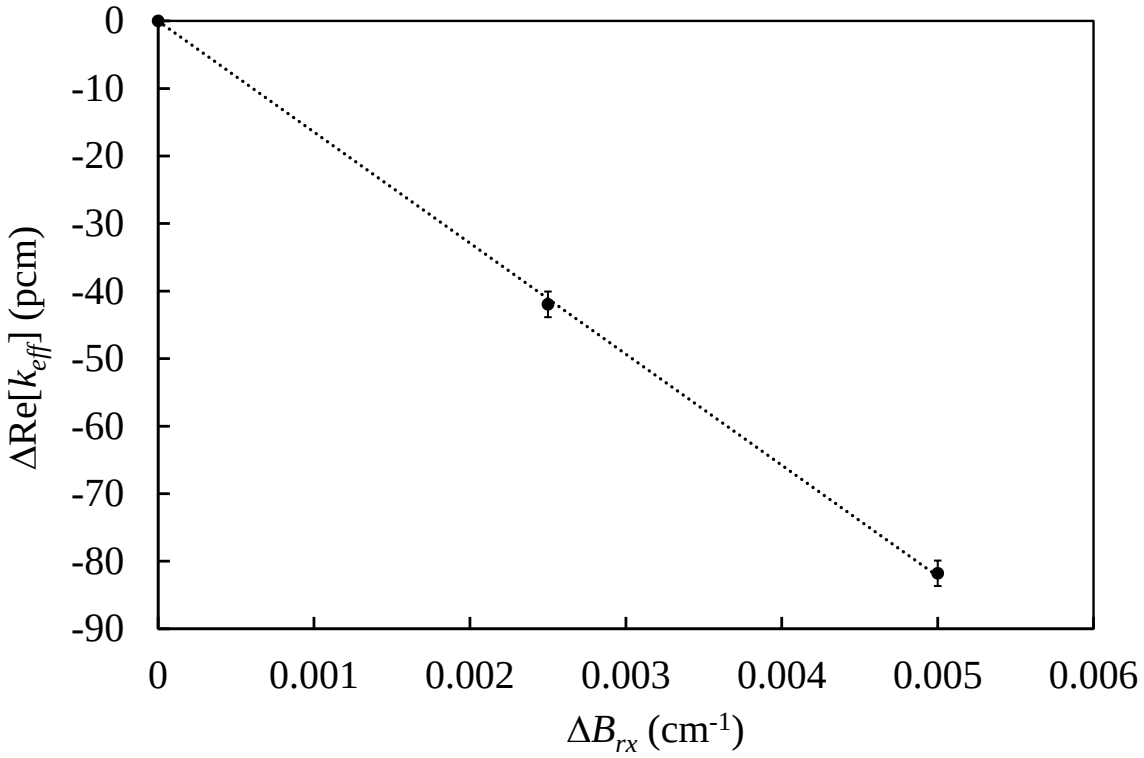

Fig. 7 ΔRe[k_{eff}] as a function of ΔB_{rx} in the asymmetric cell.

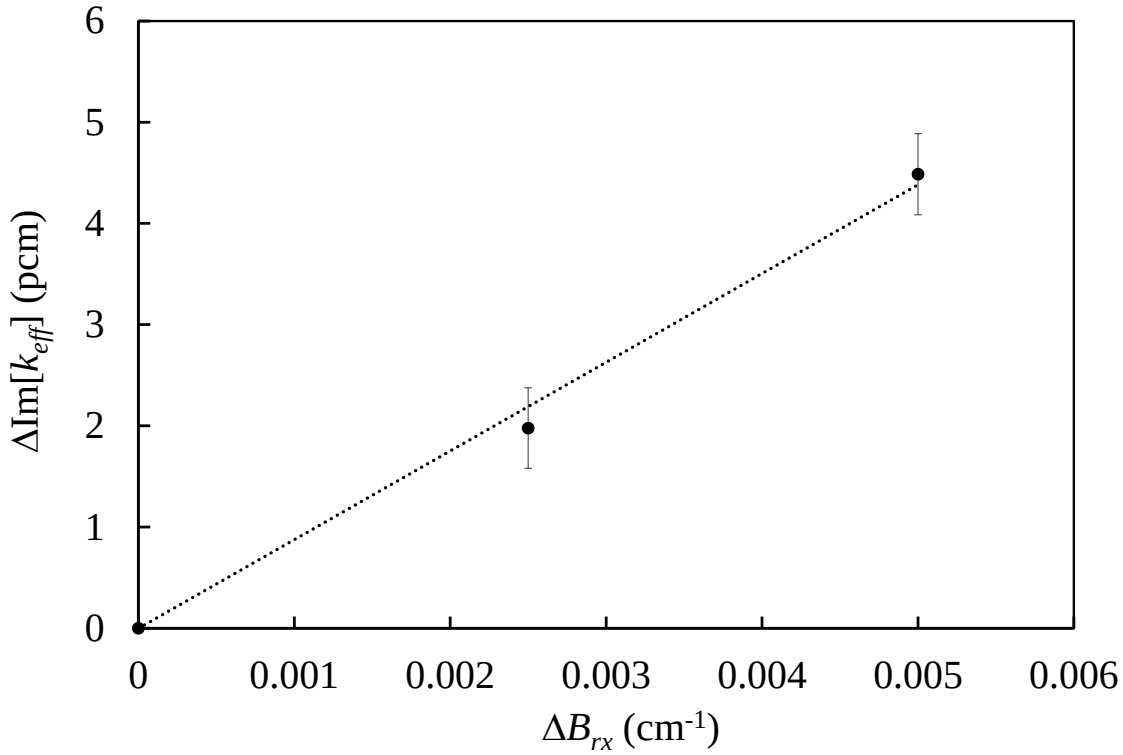

Fig. 8 ΔIm[k_{eff}] as a function of ΔB_{rx} in the asymmetric cell.

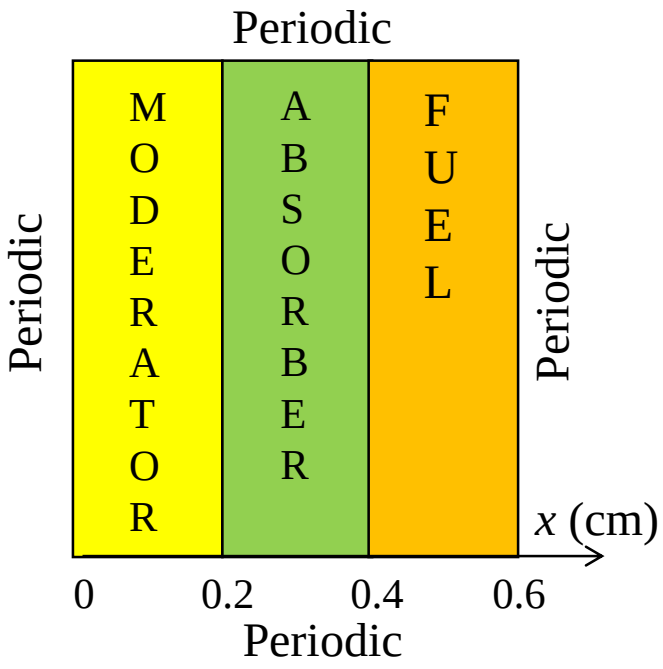

Fig. 9 Asymmetric unit cell for the test problem.

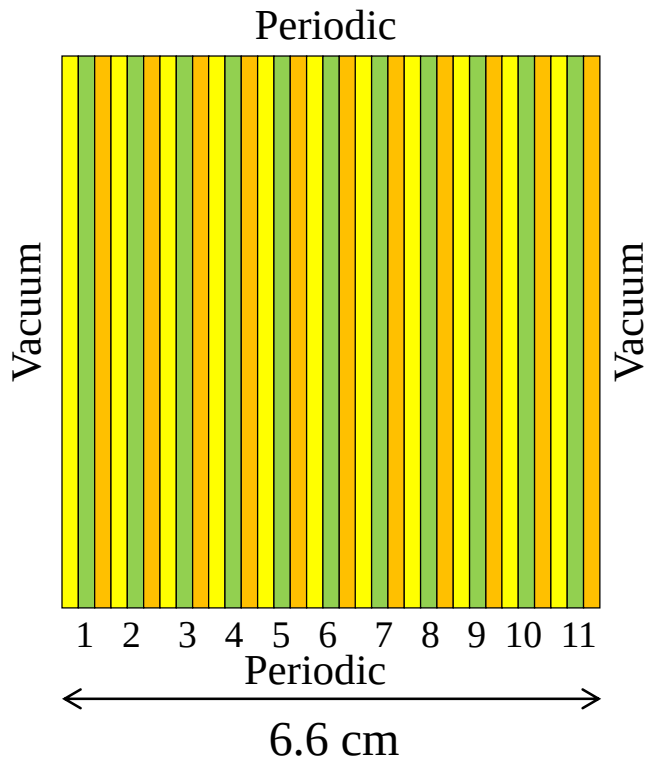

Fig. 10 One-dimensional finite slab composed of the unit cell in Fig. 9.

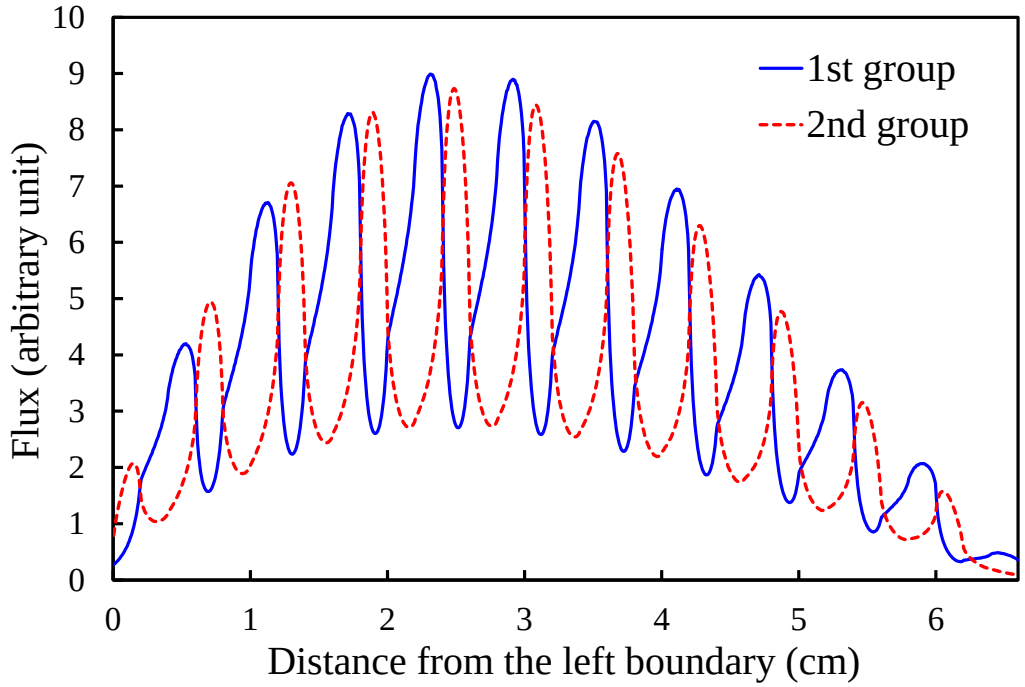

Fig. 11 Flux distributions in the one-dimensional finite slab.

Table

Table 1 Two-group constants for the one-dimensional slab (Tommasi, 2015)

		Moderator	Absorber	Fuel
Total cross section	Σ_{t1} (cm^{-1})	1.01	0.0	0.0
	Σ_{t2} (cm^{-1})	1.0	10.0	10.0
Production cross section	$\nu\Sigma_{f1}$ (cm^{-1})	0.0	0.0	0.0
	$\nu\Sigma_{f2}$ (cm^{-1})	0.0	0.0	17.365* (23.875)**
Absorption cross section	Σ_{a1} (cm^{-1})	0.0	0.0	0.0
	Σ_{a2} (cm^{-1})	0.2	10.0	10.0
Group transfer cross section	$\Sigma_s^{1\to1}$(cm^{-1})	0.01	0.0	0.0
	$\Sigma_s^{1\to2}$(cm^{-1})	1.0	0.0	0.0
Fission spectrum	χ_1	–	–	1.0
	χ_2	–	–	0.0

*for the symmetric cell in Fig. 3

**for the asymmetric cell in Fig. 6

Table 2 Critical bucklings and k_{eff} for the 1D symmetric slab.

	Buckling (cm^{-1})	Re[k_{eff}]
Monte Carlo	0.10609 ± 0.00018	0.99985± 0.00005
S_n code (Tommasi, 2015)	0.10650	0.99978

Table 3 Two-group constants for the two-dimensional square.

		Moderator	Fuel
Total cross section	Σ_{t1} (cm^{-1})	0.1	1.0
	Σ_{t2} (cm^{-1})	0.2	2.0
Production cross section	$\nu\Sigma_{f1}$ (cm^{-1})	0.0	0.0
	$\nu\Sigma_{f2}$ (cm^{-1})	0.0	0.75079
Absorption cross section	Σ_{a1} (cm^{-1})	0.0	0.07
	Σ_{a2} (cm^{-1})	0.0	0.38
Group transfer cross section	$\Sigma_s^{1\to1}$(cm^{-1})	0.06	0.651
	$\Sigma_s^{1\to2}$(cm^{-1})	0.04	0.279
Fission spectrum	χ_1	–	1.0
	χ_2	–	0.0

Table 4 Diffusion coefficients.

	1st group	2nd group
Horizontal (cm)	0.56954 ± 0.00008	0.29698 ± 0.00006
Vertical (cm)	0.59894 ± 0.00009	0.37262 ± 0.00008
Isotropic (cm)	0.59987 ± 0.00009	0.29993 ± 0.00008

Table 5 ϕ_1/ϕ_2 in the moderator.

Cell No.*	2D calculation	Critical buckling search
1	1.760	
2	1.415	
3	1.379	
4	1.362	
5	1.361	
6	1.357	1.357
7	1.360	
8	1.358	
9	1.362	
10	1.381	
11	1.428	

*The cell number is shown in Fig. 5.

Table 6 ϕ_1/ϕ_2 in the fuel.

Cell No.*	2D calculation	Critical buckling search
1	1.583	
2	1.479	
3	1.459	
4	1.453	
5	1.450	
6	1.448	1.448
7	1.450	
8	1.454	
9	1.460	
10	1.486	
11	1.636	

*The cell number is shown in Fig. 5.

Table 7 Two-group constants for the homogenized cell.

		Critical buckling	No leakage
Total cross section	Σ_{t1} (cm^{-1})	0.56439	0.55568
	Σ_{t2} (cm^{-1})	1.0995	1.11136
Production cross section	$\nu\Sigma_{f1}$ (cm^{-1})	0.0	0.0
	$\nu\Sigma_{f2}$ (cm^{-1})	0.37520	0.38013
Absorption cross section	Σ_{a1} (cm^{-1})	0.036119	0.035442
	Σ_{a2} (cm^{-1})	0.18990	0.19240
Group transfer cross section	$\Sigma_s^{1\to1}$(cm^{-1})	0.36495	0.35923
	$\Sigma_s^{1\to2}$(cm^{-1})	0.16332	0.16101

Table 8 k_{eff} and the ratios of the vertical leakage to the horizontal leakage calculated with the three methods.

		Diffusion (anisotropic)	Monte Carlo	Diffusion (isotropic)
k_{eff}		0.99676	1.00012 ± 0.00003	1.00560
L_h/L_v	1st group	1.0467	1.0241 ± 0.0002	1.0
	2nd group	1.1421	1.1339 ± 0.0002	1.0

Table 9 Sensitivity coefficients calculated by DOS and linear fitting.

	DOS	Reference
$\frac{\partial}{\partial B_{rx}}\mathrm{Re}[k_{eff}], \frac{\partial}{\partial B_{ix}}\mathrm{Im}[k_{eff}]$	−0.16295 ± 0.00005	−0.1635 ± 0.0038
$\frac{\partial}{\partial B_{rx}}\mathrm{Im}[k_{eff}], -\frac{\partial}{\partial B_{ix}}\mathrm{Re}[k_{eff}]$	0.00815 ± 0.00003	0.00897 ± 0.0081

Table 10 Critical bucklings and k_{eff} for the 1D asymmetric slab in Tommasi (2015).

	B_{rx} (cm^{-1})	B_{ix} (cm^{-1})	Re[k_{eff}]	Im[k_{eff}]
Monte Carlo	0.10689 ± 0.00013	−0.14566 ± 0.00003	0.99994 ± 0.00006	0.00004 ± 0.00001
S_n code (Tommasi, 2015)	0.10703	−0.14870	0.99978	−0.00046

Table 11 Two-group constants for the 1D asymmetric slab in Sec. 4.2.

		Moderator	Absorber	Fuel
Total cross section	Σ_{t1} (cm^{-1})	5.0	1.0	1.0
	Σ_{t2} (cm^{-1})	10.0	3.0	3.0
Production cross section	$\nu\Sigma_{f1}$ (cm^{-1})	0.0	0.0	0.0
	$\nu\Sigma_{f2}$ (cm^{-1})	0.0	0.0	5.0127
Absorption cross section	Σ_{a1} (cm^{-1})	0.0	0.2	0.0
	Σ_{a2} (cm^{-1})	0.0	3.0	2.0
Group transfer cross section	$\Sigma_s^{1\to1}$(cm^{-1})	0.0	0.8	1.0
	$\Sigma_s^{1\to2}$(cm^{-1})	5.0	0.0	0.0
Fission spectrum	χ_1	–	–	1.0
	χ_2	–	–	0.0

Table 12 Critical bucklings and k_{eff} for the asymmetric unit cell.

B_{rx} (cm^{-1})	0.45154 ± 0.00010
B_{ix} (cm^{-1})	0.15551 ± 0.00004
Re[k_{eff}]	0.999983 ± 0.000029
Im[k_{eff}]	0.000005 ± 0.000011

Table 13 ϕ_1/ϕ_2 in the moderator.

Cell No.*	1D calculation	Critical buckling search
	ϕ_1/ϕ_2	Re[ϕ_1]/Re[ϕ_2]
1	0.4221	
2	0.4486	
3	0.4466	
4	0.4456	
5	0.4451	
6	0.4446	0.4444
7	0.4440	
8	0.4436	
9	0.4428	
10	0.4419	
11	0.4440	

*The cell number is shown in Fig. 10.

Table 14 ϕ_1/ϕ_2 in the absorber.

Cell No.*	1D calculation ϕ_1/ϕ_2	Critical buckling search Re[ϕ_1]/Re[ϕ_2]
1	2.141	
2	1.900	
3	1.818	
4	1.775	
5	1.741	
6	1.713	1.720
7	1.684	
8	1.651	
9	1.600	
10	1.512	
11	1.204	

*The cell number is shown in Fig. 10.

Table 15 ϕ_1/ϕ_2 in the fuel.

Cell No.*	1D calculation ϕ_1/ϕ_2	Critical buckling search Re[ϕ_1]/Re[ϕ_2]
1	2.227	
2	2.253	
3	2.264	
4	2.270	
5	2.275	
6	2.281	2.274
7	2.288	
8	2.293	
9	2.303	
10	2.334	
11	3.295	

*The cell number is shown in Fig. 10.